Optimization of composition and obtainment parameters of biocompatible nanoemulsions intended for intraductal administration of piplartine (piperlongumine) and mammary tissue targeting

Vanessa F.M. Carvalho[1], Giovanna C. Salata[1], Jenyffer K. R. de Matos[1], Sandra Costa-Fernandez[1], Marlus Chorilli[2], Alexandre A. Steiner[3], Gabriel L. B. de Araujo[4], Edilberto R. Silveira[5], Leticia V. Costa-Lotufo[1], Luciana B. Lopes[1*]

[1] Department of Pharmacology, Institute of Biomedical Sciences, University of São Paulo, São Paulo, SP, Brazil
[2] School of Pharmaceutical Sciences at Araraquara, São Paulo State University, Araraquara, SP, Brazil
[3] Department of Immunology, Institute of Biomedical Sciences, University of São Paulo, São Paulo, SP, Brazil
[4] School of Pharmaceutical Sciences, University of São Paulo, São Paulo, SP, Brazil
[5] Department of Inorganic and Organic Chemistry, Federal University of Ceará, Fortaleza, CE, Brazil

* to whom correspondence should be addressed:

Luciana B. Lopes, PhD

Department of Pharmacology, Institute of Biomedical Sciences

University of São Paulo

Av. Prof. Lineu Prestes 1524, São Paulo - SP, Brazil

lublopes@usp.br

phone: 55 11 30917232

Abstract

As a new strategy for treatment of ductal carcinoma *in situ*, biocompatible and bioadhesive nanoemulsions for intraductal administration of the cytotoxic agent piplartine (piperlongumine) were optimized in this study. To confer bioadhesive properties, the nanoemulsion was modified with chitosan or hyaluronic acid. Tricaprylin was selected as the nanoemulsion non-polar phase due to its ability to dissolve larger drug amounts compared to isopropyl myristate and monocaprylin. Use of phosphatidylcholine as sole surfactant did not result in a homogeneous nanoemulsion, while its association with polysorbate 80 and glycerol (in a surfactant blend) led to the formation of nanoemulsions with droplet size of 76.5 ± 1.2 nm. Heating the aqueous phase to 50°C enabled sonication time reduction from 20 to 10 min. Inclusion of either chitosan or hyaluronic acid resulted in nanoemulsions with similar *in vitro* bioadhesive potential, and comparable ability to prolong mammary tissue retention (to 120 h) *in vivo* without causing undesirable histological alterations. Piplartine was stable in both nanoemulsions for 60 days; however, the size of loaded NE-HA was maintained at a similar range for longer periods of time, suggesting that this nanoemulsion may be a stronger candidate for intraductal delivery.

Key words: nanoemulsion, bioadhesion, breast cancer, piplartine, intraductal delivery

INTRODUCTION

Ductal carcinoma *in situ* (DCIS) is a type of breast cancer characterized by cell proliferation without evidence of invasion in the basal membrane and adjacent tissue (Fallowfield and Francis, 2016). It accounts for approximately 20% of nonpalpable breast tumors diagnosed with mammography (Sagara et al., 2015; Ward et al., 2015). Because of its heterogeneity, it is estimated that 25-50% of the lesions may progress to invasive disease (Benson et al., 2016); thus, DCIS management has traditionally followed the standard of care of invasive breast cancer: surgical excision, radiation therapy and/or oral tamoxifen for estrogen-positive tumors (Groen et al., 2017; Sagara et al., 2015). However, recent studies demonstrated that this standard of care does not influence mortality related to subsequent invasive forms of the disease (Fallowfield and Francis, 2016; Narod et al., 2015), emphasizing the need to consider biological markers and other characteristics to diagnose low-risk lesions and enable the use of less aggressive treatment approaches (Benson et al., 2016; Campbell et al., 2017; de Groot et al., 2016).

More recently, administration of cytotoxic drugs directly into the mammary ducts has been described as a new option for local treatment and chemoprevention of precursor and atypical lesions, DCIS, and as a neoadjuvant treatment option prior to surgery (Love et al., 2013; Murata et al., 2006). Preclinical data have shown the feasibility of the intraductal route for administration of chemotherapeutic agents such as paclitaxel and doxorubicin in rodents with significant reduction of tumor development and incidence of systemic drug adverse effects in N-methyl-N-nitrosourea-induced models, spontaneously arising Her2/*neu*transgenic mouse models and other mammary tumor models (Gu et al., 2018; Murata et al., 2006; Okugawa et al., 2005; Stearns et al., 2011). Intraductal administration has also been performed in clinical settings for drug delivery (Love et al., 2013). For example, Stearns *et al*. were able to cannulate the most visible ductal orifice in volunteers (Stearns et al., 2011). Mahoney *et al*. demonstrated the feasibility of cannulating a specific DCIS-containing duct in women and instilling a cytotoxic agent before

77 breast cancer surgery (Mahoney et al., 2013). Carboplatin or pegylated liposomal doxorubicin
78 (PLD) was administered into five to eight ducts at three dose levels in women awaiting
79 mastectomy (Love et al., 2013). Intraductal administration was generally well tolerated with mild,
80 transient breast discomfort, and mean of pain ranging from 0.2 to 1.2 (on a 10-point scale) after
81 local application of lidocaine (Stearns et al., 2011; Zhang et al., 2014). Plasma drug levels were
82 lower than after intravenous administration, supporting the relevance of intraductal
83 administration for local treatment (Stearns et al., 2011).

84 Although intraductal administration has attracted interest, there is a need for specific
85 formulations designed for this route, characterized by biocompatibility and ability to prolong
86 drug retention in the mammary tissue. In a previous study, we have developed a nanoemulsion
87 using polysorbate 80 as sole surfactant, and demonstrated its feasibility for intraductal
88 administration (Migotto et al., 2018). Building upon our previous study, our first goal in this
89 study was to optimize the composition and production parameters of nanoemulsions for
90 intraductal delivery of the cytotoxic drug piplartine. Also known as piperlongumine, piplartine is
91 an alkaloid of *Piper* species that demonstrated cytotoxic and antiproliferative activity against
92 several tumor cell lines including prostate, colon, breast and melanoma (Bezerra et al., 2007;
93 Bezerra et al., 2008b; Kong et al., 2008; Raj et al., 2011; Tsai et al., 2005). Piplartine induces
94 DNA damage, leading to cell death by apoptosis and necrosis depending on concentration
95 (Bezerra et al., 2007), and G2/M cell cycle arrest followed by mitochondrial-dependent apoptosis
96 (Bezerra et al., 2013).

97 To optimize nanoemulsion composition and production parameters, we established ideal
98 formulation attributes (based on the administration route), identified factors that might influence
99 these attributes, and investigated the influence of each factor while keeping others constant. The
100 nanoemulsion attributes included (i) size ≤ 100 nm at the time of obtainment to avoid any risk of
101 duct obstruction, which was defined based on ducts dimensions (0.5-2 mm), (ii) PDI < 0.3 to

ensure low polydispersity and homogeneous size distribution, and (iii) bioadhesive properties, obtained by nanocarrier modification with a cationic (chitosan) or anionic (hyaluronic acid) polymer, enabling comparison of the influence of type and charge of the bioadhesive polymer (Ferris-James et al., 2012; Loureiro et al., 2015; McClements, 2012; Migotto et al., 2018). Chitosan has been described to adhere to mucous membranes mainly due to electrostatic interactions with negatively charged surfaces (Mazzarino et al., 2012; Smart, 2005), while hyaluronic acid is a major component of the extracellular matrix and major ligand of CD44 and RHAMM receptors, which are overexpressed on a variety of tumor cell surfaces (including in the breast) (Akima et al., 1996; Guter and Breunig, 2017).

Following optimization of the nanoemulsion composition and production parameters, our second goal was to compare the characteristics and properties of selected nanoemulsions modified with chitosan and hyaluronic acid. Characteristics and properties of interest that were studied included irritation potential, rheological and bioadhesive properties, in addition to stability, drug release, *in vivo* retention and local histological alterations.

MATERIAL AND METHODS

Material

Polysorbate 80, DMSO, low molecular weight chitosan (50,000-190,000 Da), hyaluronic acid (130,000-150,000 Da), and propylene glycol were obtained from Sigma (St. Louis, MO, USA). Glycerol was purchased from Synth (Diadema, SP, Brazil). Tricaprylin was kindly supplied by Abitec Corporation (Janesville, WI, USA). Acetonitrile, ethanol and methanol were purchased from Mallinckrodt Baker (Phillipsburg, NJ, USA). Soy phosphatidylcholine (PC) was purchased from Avanti Polar Lipids (Alabaster, AL, USA). Ultra-pure water was used unless stated in the individual methods. Piplartine was isolated from roots of *Piper tuberculatum*, harvested from the Campus of Federal University of Ceará (Fortaleza, CE, Brazil; voucher

specimen #34736 deposited at Prisco Bezerra herbarium, Federal University of Ceará) and characterized as previously described (Bezerra et al., 2007). Briefly, ground roots (420.0 g) were macerated with petroleum/ethyl acetate (1:1, v/v) thrice for 24 h; the solvent was evaporated under reduced pressure to yield a yellowish solid, and piplartine was crystallized with methanol. Characterization was performed by 1D and 2D NMR analyses and melting point determination as previously described (Bezerra et al., 2008a; Bezerra et al., 2008b).

Methods

1. Oil phase selection

The oil phase of the nanoemulsion was selected based on piplartine solubility, which was determined by adding 2-4 mg of the drug to 200 mg of tricaprylin, isopropyl myristate, monocaprylin and tricaprylin:monoolein (3:1), followed by stirring for 2 hours at 25 ± 2 °C (Fofaria et al., 2016; Qhattal et al., 2011). Our goal was to find oil phase components in which piplartine could be dissolved in up to 0.5 h to avoid a lengthy nanoemulsion preparation process. After bath sonication for 10 min (piplartine remains stable after sonication) (Carvalho et al., 2019), samples were centrifuged at 2600xg for 10 min, and presence of sediment and/or drug crystals were assessed by visual inspection and optical microscopy. Based on the absence of sediment when piplartine was dissolved in tricaprylin at the highest concentration, this triglyceride was selected as the oil phase. In addition to providing drug solubilization, another advantage of tricaprylin is that it is considered safe for parenteral administration (Floyd, 1999).

2. Nanoemulsion development and optimization

Soybean phosphatidylcholine (PC) was used as sole surfactant or partially replaced with polysorbate 80 to obtain nanoemulsions. Glycerol was investigated as a co-surfactant due to its

ability to reduce the diameter of aggregates and promote homogeneous size distribution (Carvalho et al., 2017b; Ochoa-Flores et al., 2017).

The PC, tricaprylin and water ratios necessary to obtain nanoemulsions were established using previously described pseudo-ternary phase diagrams (Patel et al., 2006). The PC content was set at < 20%, while the aqueous phase content was set at 60% or higher. For formulations containing PC, polysorbate and glycerol as surfactant blend (at 3:1:0.5, w/w/w), pseudo-ternary phase diagrams were obtained by mixing this blend with tricapylin at 8:2 to 2:8 (w/w), followed by titration with water at 10-20% increments. The relationship between phase behavior and composition was demonstrated in a phase diagram (**Supplementary Figure 1**). Because they enabled the obtainment of milky and dispersed systems, surfactant blend:oil phase ratios of 2:1 and 1:1 (m/m), and aqueous phase content over 60% were selected.

To obtain nanoemulsions, the oil phase (tricaprylin) was combined with the surfactant blend prior to aqueous phase addition, which was composed of a PBS solution containing poloxamer, chitosan or hyaluronic acid. Because chitosan dissolves at pH<5, an aqueous solution of chitosan in water acidified to pH=4.5 was prepared, and added to PBS for a final concentration of 1%. The system was homogenized by vortex mixing (30 s), followed by sonication for 5-20 min with pulses of 58 s every 30 s in ice bath using 40% maximum amplitude (VCX500, Sonics, Newtown, CT, USA) (Migotto et al., 2018).

To optimize nanoemulsion production, variations were introduced to this protocol, and four sets of experiments were conducted as described below. Three to four batches of each formulation were produced for comparison of size and zeta potential.

2.1. Influence of surfactant composition and aqueous phase content: the surfactant (PC or PC:polysorbate 80:glycerol at 3:1:0.5, w/w/w) was mixed with tricaprylin at 1:1 or 2:1 (w/w),

175 followed by addition of PBS as aqueous phase at 66-80%, homogenization by vortex-mixing and
176 sonication for 20 min.
177
178 ***2.2. Influence of poloxamer 407:*** because poloxamer has been described to aid emulsification,
179 improve droplet size distribution and provide steric stability (Loureiro et al., 2015; Mistry et al.,
180 2012), the influence of its concentration on nanoemulsion characteristics was assessed. The
181 surfactant blend (PC:polysorbate 80:glycerol, 3:1:0.5, w/w/w) was combined with tricaprylin at
182 1:1 (w/w), followed by addition of PBS (80%) containing poloxamer 407 to yield final
183 concentrations of 0-0.5% (w/w); the system was subsequently subjected to homogenization and
184 sonication for 20 min.
185
186 ***2.3. Influence of aqueous phase temperature and bioadhesive polymer addition on sonication***
187 ***time:*** the surfactant blend (PC:polysorbate 80:glycerol, 3:1:0.5, w/w/w) was combined with
188 tricaprylin at 1:1 (w/w), followed by addition of PBS containing chitosan (1%) or hyaluronic acid
189 (1%) as aqueous phase (80%). The aqueous phase was either used at room temperature
190 (maintained at 25 °C by air conditioning) or heated (50 °C in water bath) prior to addition to the
191 surfactant:oil phase mixture and sonication for 5-20 min. Selected nanoemulsions modified with
192 hyaluronic acid and chitosan will be referred to as NE-HA and NE-Q, respectively.
193
194 ***2.4. Influence of cetylpyridinium chloride on nanoemulsion charge:*** because nanocarrier charge
195 affects interaction and drug penetration into other tissues, with a positive charge favoring
196 interaction with biological barriers (Pepe et al., 2013), we also attempted to produce a cationic
197 hyaluronic acid-modified nanoemulsion by including cetylpiridinium chloride as a co-surfactant.
198 This approach derived from previous studies that employed small amounts of positively charged
199 amphiphilic molecules to ensure the interaction of the interface with the negatively charged

hyaluronate (Pereira et al., 2016). Tricaprylin was combined with the surfactant blend containing cetylpyridinium chloride (to obtain final concentrations in the nanoemulsion of 0.1-0.5%) followed by addition of 80% aqueous phase containing hyaluronic acid (1%, heated at 50 °C). The mixtures were homogenized by vortex mixing (30 s) followed by sonication for 10 min (as defined in experiment 2.3). The nanoemulsion modified with cetylpyridinium chloride will be referred to as NE-CET.

3.1. Characterization and evaluation of selected nanoemulsion properties

Size and zeta potential were determined using Zetasizer NanoZS90 equipment (Malvern, UK) after nanoemulsion dilution with water at 1:100 (w/w). Size and zeta potential of samples from different batches (3-4) were measured within 20 min from obtainment.

3.2. Rheological behavior

The influence of the bioadhesive polymer to the nanoemulsion rheological behavior and viscosity was evaluated using a R/S Plus controlled stress rheometer with RC75-1 cone (Brookfield Engineering laboratories, Middleboro, MA), and a bath circulator for temperature control, set at 25°C under shear rate control conditions within the range 1–500 s^{-1} (Carvalho et al., 2017a). Rheograms of shear stress were recorded against shear rate, and the data fitted to Power Law model according to the following equation: $\tau = K\, g^n$, where τ is the shear stress, g is the rate of shear, K is the consistency index and n is the flow index parameter, used to classify the rheological behavior. According to n, fluids were classified as Newtonian when $n = 1$, whereas $n > 1$ or $n < 1$ indicates shear-thickening or shear-thinning, respectively (Hosmer et al., 2013).

3.3. Morphological characterization

The structure and morphological aspect of selected nanoemulsions was assessed using transmission electron microscopy (TEM; FEI Tecnai G20 20 XTWIN, France) at an acceleration voltage of 100 kV. A 2% solution of phosphotungstic acid (PTA) was prepared and adjusted to pH 7.4 using a sodium hydroxide solution. To 1 mL of a nanoemulsion suspension, 1 mL of PTA was added, and the sample was adsorbed onto carbon film on 300 mesh copper grids and dried at room temperature prior to microscopic analysis.

3.4. DSC analysis and glass transition temperature

To learn more about the interaction of chitosan and hyaluronic acid with the nanoemulsion, the glass transition temperature and thermal behavior of NEQ and NEHA were assessed by differential scanning calorimetry (DSC) using a Discovery DSC 2500 (TA Instruments, New Castle, DE) equipped with a RCS90 cooling system. NE without bioadhesive polymers was used for comparison. Samples of 8-10 mg were placed in Tzero® aluminum pans (TA Instruments, New Castle, DE, USA), hermetically sealed, equilibrated at 20 °C, and submitted to measurements in two steps: cooling from 20 to - 80 °C at 10 °C/min, and heating to 40 °C at 20 °C/min. Nitrogen was used as a purge gas (25 mL/min) and an empty pan was used as a reference. Data collection and determination of thermal properties were performed using the TRIOS Software v4.5.0 (TA Instruments, New Castle, DE).

4. Irritation potential

To investigate the relationship between nanoemulsion composition and irritation potential, Hen's Egg Test—Chorioallantoic Membrane (HET-CAM) was used following previously published guidelines and studies (ECVAM DB-ALM, INVITOX protocol 96) (Contri et al., 2016; McKenzie et al., 2015; Migotto et al., 2018). The protocol was conducted in accordance with the guidelines from the Brazilian Council for Control of Animal Experimentation

(CONCEA), and approved by the Animal Care and Use Committee (IACUC) at the Institute of Biomedical Sciences of the University of São Paulo (protocol number 70/2016, São Paulo, Brazil). Fertilized chicken eggs (obtained from Sabor Natural, São Paulo, SP, Brazil) were incubated for 9 days at 37°C and 55% humidity (Premium Ecologica incubators, Belo Horizonte, MG, Brazil) with automatic rotation every 2 h. The chorioallantoic membrane was exposed and treated for 5 min with selected nanoemulsions, saline (negative control) and NaOH (0.1M, positive control); they were photodocumentated (Nikon, SMZ 1500, Tokyo, Japan) before, during and after treatment. Each treatment was performed in 5-6 eggs, and a score was calculated using the following equation as previously described (Mojeiko et al., 2019).

$$II= ((301-h)/300)x5 + ((301-l)/300)x7 + ((301-c)/300)x9$$

where h, l and c are the time (in seconds) of the beginning of hemorrhage, lysis or coagulation. The following classification was used: $II< 0.9$: non-irritant; $1 < II < 4.9$: slight irritation; $5.0 < II < 8.9$: moderate irritation; $9.0 < II < 21$: severe irritation (Luepke, 1985).

5. In vitro bioadhesion assessment

To compare the impact of chitosan and hyaluronic acid on the bioadhesive properties of the nanoemulsion, we assessed interactions between the nanoemulsions and the subcutaneous tissue of porcine ear skin (as model for the mammary tissue) using TA-XTplus texture analyzer (Stable Micro Systems, Surrey, UK). We acknowledge the differences between the subcutaneous and mammary tissues, but use of porcine skin allowed us to comply with the Institutional Animal Care and Use (IACUC) 3Rs guidelines since it is commercially available and considered exempt from IACUC review and approval. Fresh porcine ear skin was obtained from a local slaughterhouse, and the skin from the outer side of the ear was removed with a scalpel and scissors while keeping the subcutaneous tissue attached to the skin (Lopes et al., 2009; Thomas et al., 2014). Skin sections were frozen at −80°C until the day of the experiment.

For assessment of bioadhesion potential, the skin was attached to the lower end of a cylindrical probe (diameter 10 mm) with a rubber ring (Bento da Silva et al., 2017), with the subcutaneous tissue facing outside (for contact with formulations) to mimic the mammary tissue. The probe was lowered at constant speed (1 mm/s) to make contact with the surface of the nanoemulsions (NE-HA and NE-Q). The skin and the sample were kept in contact for 60 s without any force applied, after which the probe rose at a constant speed (0.5 mm/s) until the contact between the surfaces was broken. The bioadhesive force of the formulations was measured as the maximum detachment force or the resistance to the withdrawal of the probe. The experiment was repeated 6 times for each sample. Because of the low viscosity and high aqueous content of the nanoemulsions, the force necessary to detach water was measured for comparison.

6. In vivo intraductal administration, mammary tissue targeting and histological assessment

This experiment aimed at comparing the (i) localization of a fluorescent marker in the mammary tissue mediated by intraductal and systemic (i.p.) administration of nanoemulsions, (ii) influence of the type and charge of the bioadhesive polymer on the nanoemulsion ability to prolong mammary tissue, and (iii) nanoemulsion advantage over a simple solution. NE-Q and NE-HA containing Alexa Fluor 647 (0.05%, w/w) as a fluorescent marker were prepared by dilution in the aqueous phase prior to nanoemulsion sonication and formation. Following intraductal or intraperitoneal (i.p.) administration, whole body animal imaging was used to track fluorescence distribution. To ensure that fluorescence was related to Alexa fluor presence in the tissue, unloaded nanoemulsions were administered as controls.

Female Wistar rats from the Facility for SPF rat production at the Institute of Biomedical Sciences - Animal Facility Network at University of São Paulo - were housed in the Animal Facility of the Department of Pharmacology with free access to food and water until they reached 250 ± 20 g. The animal room was kept under a 12:12 h light–dark cycle (lights on at 7:00 am),

and temperature was maintained between 22-23°C. The protocol was conducted in accordance with guidelines issued by the Brazilian Council for Control of Animal Experimentation (CONCEA), and approved by the Animal Care and Use Committee of the Institute of Biomedical Sciences at University of São Paulo (protocol number 69/2016, São Paulo, Brazil).

Briefly, rats were anaesthetized with isoflurane (5% for induction and 2.5% for maintenance, Cristalia, Itapira, Brazil), and abdominal hair was removed using a depilatory cream (Migotto et al., 2018). Twenty four hours after hair removal, animals were divided in 7 groups based on the treatment they were going to receive: intraductal (i) saline, (ii) unloaded NE-Q, (iii) unloaded NE-HA, (iv) Alexa fluor solution (PBS:propylene glycol, 1:1), (v) Alexa fluor-loaded NE-Q, or (vi) Alexa fluor-loaded NE-HA, and intrerinoteal (i.p.) (vii) Alexa-fluor loaded NE-HA (4 animals/group were used, with the exception of group vii that contained 3 animals).

The treatments were delivered under anesthesia with isoflurane as follows. First, the nipples were gently rubbed with alcohol to reveal the duct orifice (Chun et al., 2012; Krause et al., 2013). Three pairs of nipples were selected according to their ease of access, and under a dissection microscope, 10 μL of the drug solution or the nanoemulsions was injected into the orifice using a 33 G needle attached to a Hamilton syringe (Hamilton, Bonaduz, Switzerland). Saline was administered as a control formulation to assess mammary tissue damage.

Distribution of Alexa fluor was monitored for 1-120 h using a whole body bioimaging system (IVIS Spectrum System, Perkin-Elmer Life Sciences, Waltham, MA, USA). The following instrument settings were fixed for comparison among groups: exposure time= 5 s, binning factor= 8, excitation/emission= 465/540 nm.

To assess histological changes induced by the formulations, mammary glands from animals treated with unloaded nanoemulsions or saline were excised 120 h post-injection, fixed in 10% buffered neutral formaldehyde and processed for inclusion in paraffin (Murata et al., 2006). Histological sections of 5 μm were obtained, and stained with hematoxylin/eosin prior to

microscopic analyses. Presence of tissue edema, infiltration of inflammatory cells and changes in the morphology of ducts and lobular units were investigated to assess formulation-induced histological alterations (Chun et al., 2012).

7. Incorporation of piplartine and in vitro release

Piplartine was dissolved in the surfactant-oil phase mixture to obtain a final concentration of 1% (w/w) prior to addition of the aqueous phase. This concentration was 2-fold smaller than the maximum amount that could be dissolved, suggesting that drug concentration in the nanocarrier would be below saturation, and avoiding the influence of formulation saturation and supersaturation on drug release (Brewster et al., 2008; Land et al., 2006).

The *in vitro* release of piplartine was evaluated using Franz diffusion cells and phosphate-buffered receptor phase (100 mM, pH 7.2) containing 20% ethanol under constant stirring (350 rpm) at 37.0 ± 0.5 ° C (Cichewicz et al., 2013). Ethanol was added to aid drug solubility (Carvalho et al., 2019; Hosmer et al., 2013). Other receptor phase additives were tested, such as poloxamer 407 (1%), polysorbate 80 (1%) or BRIJ 97 (1%), but ethanol addition led to a more pronounced increase (at least 1.7-fold) in drug solubility. Previous studies have employed ethanol at higher percentages to overcome the low aqueous solubility of lipophilic drugs, and a comparison of its content (38 or 76%) revealed that it exerted no significant influence on the release rate (Rege et al., 1998; Solomon et al., 2012). The stirring speed was selected based on preliminary experiments that compared drug release from NE-HA when the receptor phase was stirred at 200 or 350 rpm. A similar cumulative drug release at 16 h was observed at 200 and 350 rpm; however a 350 rpm speed was selected, as higher speeds are recommended in experiments employing Franz diffusion cells (Praca et al., 2018). Similar observations were reported in clomipramine release studies comparing receptor phase stirring at 200 and 400 rpm (Richter et al., 1969).

A cellulose membrane (1000 Da cut, Sigma, St. Louis, MO) was placed between the recipient and donor compartments and 100 μL of the nanoemulsion was added in the donor compartment. The receptor phase (300 μL) was collected at 1, 2, 4, 6, 8 and 16 h post-application, and the same volume was replaced. The 16 h time point was selected as the latest because drug concentration in the receptor phase reached 80% of its solubility; thus, we acknowledge that sink condition was not maintained during the whole experiment, but as stated earlier, the most pronounced increase in drug solubility was obtained with ethanol. To demonstrate that diffusion of free piplartine across the dialysis membrane is not a rate-limiting step, a drug solution in propylene glycol was used as a control formulation. The experiment was interrupted at 6 h because drug concentration in the receptor phase reached 80% of its solubility.

Piplartine in the receptor phase was quantified by HPLC as described in section 9. Interference of formulation components in the analytical method was assessed by adding unloaded formulations to the donor compartment of diffusion cells and assaying the receptor phase after 24 h; since no interference was detected at this late time point (which would enable diffusion of larger amounts of components and facilitate their detection), we assumed the same for earlier time points. To estimate the cumulative drug release, the amount of drug collected at earlier time points were added to the observed (or measured) drug amount in the receptor phase at a given time point as follows:

$$Ct_n = C_n + C_{w,}$$

where Ct_n is the corrected drug amount at a given time n, C_n is the observed drug amount in the receptor phase at a given time n, and C_w is the sum of all drug amounts withdrawn (i.e., collected at earlier time points). To calculate percentages, the total amount of drug added to the donor compartment was set as 100%. The release kinetics was determined by plotting cumulative drug release against time (for zero order kinetics), square root of time (for pseudo-first order kinetics)

and the log of remaining drug against time (for first order kinetics), and coefficients of determination were obtained (Ng et al., 2017; Phelps et al., 2011).

8. Stability study of nanoemulsions

The chemical and physical stability of unloaded and piplartine-loaded NE-HA and NE-Q were studied by macroscopic and microscopic observation taking into consideration phase separation, creaming, droplet agglomeration or sedimentation, and analysis of particle size, polydispersity index, zeta potential and piplartine content.

In a conical tube, 0.5 g of the unloaded or piplartine-loaded NE-HA and NE-Q (1% w/w) prepared in triplicate were stored at room temperature (maintained at 25°C with air conditioning) for 60 days. Formulation evaluation was performed at days 0 (immediately after production), 7, 14, 30, 45, and 60. Size and zeta potential were determined as described in *item 3.1*. Microscopic examination was conducted under halogen and polarized light (Leica, Wetzlar, Germany) to investigate the presence of drug crystals, agglomeration and phase transformation since PC and polysorbate 80 form liquid crystalline phases, which display specific textures under polarized light.

For quantification of piplartine, 10 μL of the samples were diluted in 1 mL of methanol (to yield a theoretical drug concentration of 100 μg/mL) at days 0, 7, 30, 45 and 60, and the samples were subjected to HPLC analysis as described in section 9 (Carvalho et al., 2019). To express drug content as percentage, drug concentration at day 0 was considered 100%.

9. HPLC analysis of piplartine

Chromatographic analyzes were performed using a Shimadzu HPLC system equipped with a pump (model LC-20AB), an autosampler (model SIL-20A), an UV detector (model SPD-M20A) set at 325 nm, and the Class-VP software. Piplartine separation was performed in a

Phenomenex C18 (150 × 4.6 mm) column maintained at 25°C according to a previously developed and validated method (Carvalho et al., 2019). Briefly, the mobile phase was composed of 1:1 (v/v) acetonitrile:water (pH adjusted to 4.0 with 0.1% acetic acid) and used at a flow rate of 0.9 mL/min. The calibration curve of piplartine was prepared in methanol, and demonstrated linearity within the range 0.2 - 150 μg/mL. The amount injected into the column was 20 μL for samples and calibration curve. For each experiment, new calibration curves were obtained.

10. Statistical analyses

The results are reported as means ± SD. Data were statistically analyzed using ANOVA test followed by Tukey post-hoc test (GraphPad Prism software, Sand Diego, CA). Values were considered significantly different when $p < 0.05$. ANOVA-based power analysis was conducted to estimate sample size with power at 0.90 and alpha at 0.05 (Statistica software, Palo Alto, CA).

RESULTS

1. Nanoemulsion development and optimization

The first goal of the present study was to optimize the composition and production parameters of nanoemulsions for intraductal delivery of piplartine. The influence of surfactant composition, aqueous phase content and temperature, sonication time, poloxamer and bioadhesive polymer addition on nanoemulsion formation and physicochemical characteristics such as diameter, polydispersity and zeta potential are presented below.

1.1. Influence of surfactant composition and aqueous phase content

To assess the influence of surfactant and aqueous phase content, the dispersions were sonicated for 20 min employing the aqueous phases at room temperature. Use of PC as sole

surfactant failed to form nanoemulsions; instead, viscous and turbid mixtures were obtained. Inclusion of polysorbate 80 and glycerol in the surfactant blend resulted in a fluid, translucent and opalescent dispersion, with particle diameter of 90.7 ± 1.0 nm and a slightly positive zeta potential when the aqueous phase content was 75% (**Table 1**), but its PDI was above the upper limit of the range considered acceptable for drug delivery systems (Danaei et al., 2018). A further increase in the aqueous phase content to 80% produced a 1.5-fold reduction in PDI, while size and zeta potential were not significantly altered. Because increases in aqueous content frequently results in higher drug release rates, which affects bioavailability (Chang and Bodmeier, 1997; Cichewicz et al., 2013), aqueous phase at 80% was selected for nanoemulsion preparation.

Increasing the surfactant:oil phase ratio to 2:1 (w/w) did not promote significant changes on size, despite previous reports suggesting that increasing surfactant content decreased droplet size (Lefebvre et al., 2017). Due to the risk of increasing formulation irritation often associated with surfactant content increments (Pepe et al., 2013), the 1:1 ratio was selected.

1.2. Influence of poloxamer 407

Because poloxamer has been described to aid emulsification, decrease nanoemulsion droplet size, improve size distribution and provide steric stabilization, the influence of its concentration on nanoemulsion characteristics was assessed (Loureiro et al., 2015; Mistry et al., 2012). Contrary to our expectations, poloxamer increases from 0 to 0.25 or 0.50% did not affect size or PDI in a significant manner (**Table 2**). However, the nanoemulsion containing poloxamer at 0.50% transformed into a gel within 2 months at room temperature, leading to poloxamer exclusion from the composition.

1.3. Influence of aqueous phase temperature and bioadhesive polymer addition

It has been generally advisable to limit the sonication time to reduce unanticipated sample responses to the heat generated by the process and to avoid probe-derived titanium contamination (Betts et al., 2013). Thus, the next step was to assess the influence of aqueous phase temperature and type/charge of the bioadhesive polymer on the sonication time required to produce nanoemulsions.

Nanoemulsions containing chitosan (NE-Q) or hyaluronic acid (NE-HA) were prepared by adding the aqueous phase at room temperature (25 °C maintained with air conditioning) or heated at 50°C, followed by sonication for 5-20 min. Sonication with the aqueous phase at room temperature reduced NE-Q droplet size from ~500 nm (t=0) to 185 nm after 5 min, to ~120 nm after 10 min, to ~78 nm after 15 min, and to ~74 nm after 20 min (**Supplementary Figure 2**). Heating the aqueous phase (50°C) led to size reduction to ~74 nm after 10 min of sonication, which represents a reduction of 1.7-fold compared to the non-heated aqueous phase ($p < 0.05$). Subsequent sonication pulses did not produce further changes on size. For NE-HA, sonication for 5 min reduced droplet size by ~2.5-fold ($p < 0.05$) using the heated aqueous phase compared to the non-heated system, but this difference disappeared after sonication for 10 min. PDI < 0.3 was observed after 5 min of sonication regardless of the temperature of the aqueous phase. To reduce sonication time but keep the same number of pulses for NE-Q and NE-HA, aqueous phase heating to 50°C and sonication for 10 min (using pulses of 58 s on and 30 s off) were defined as optimum parameters. The resulting zeta potential of NE-HA and NE-Q were -5.7 ± 1.7 mV and +11.3 ± 3.2 mV, respectively.

1.4. Influence of cetylpyridinium chloride

To confer a positive charge to NE-HA and take advantage of possible electrostatic interactions between cationic nanocarriers and negatively charged epithelium surfaces, cetylpyridinium chloride was included in the nanoemulsion. At 0.5%, but not at lower

472 concentrations, this surfactant led to zeta potential inversion and to the obtainment of a cationic
473 system (+11.3 mV, **Table 3**). Based on these results, cetylpyridinium chloride concentration was
474 set at 0.5% to produce NE-CET.
475
476 ***2. Characterization and evaluation of selected nanoemulsion properties***
477 Having optimized nanoemulsion composition and sonication parameters, we proceeded to
478 characterize and compare the properties of selected formulations modified with chitosan and
479 hyaluronic acid. The influence of alginate, chitosan and cetylpyridinium chloride on
480 nanoemulsion stability, irritation potential, morphology, glass transition temperature, rheological
481 and bioadhesive properties are presented below.
482
483 *2.1. Stability:* unloaded NE-Q, NE-HA and NE-CET were preliminarily screened for stability at
484 room temperature. Among these nanoemulsions, NE-Q displayed the highest variation in size,
485 which increased~1.4-fold within 60 days (**Figure 1**). In spite of this increase, no signs of phase
486 separation, creaming and/or sedimentation were observed macroscopically or microscopically,
487 and PDI values did not increase beyond 0.3 throughout the study. No pronounced changes on size
488 or PDI were observed for NE-HA or NE-CET. However, NE-CET zeta potential value decreased
489 by 2-fold after 60 days compared to initial values.
490
491 *2.2. Irritation potential*: the ability of nanoemulsions to cause tissue irritation was compared
492 using HET-CAM. Initially employed to assess eye irritation, HET-CAM use has now been
493 expanded, and it currently finds applicability as an alternative method to the use of animals to
494 estimate irritation to the skin and other tissues (Eichenbaum et al., 2013; Mehling et al., 2007).
495 Application of saline (negative control) to healthy membranes produced no perceptible change
496 over the five-minute time window (**Figure 2**), while NAOH (0.1 M, positive control) caused

lysis, coagulation and severe hemorrhage, resulting in a score of 17.9 ± 0.6, which classifies this solution as severe irritant (Fangueiro et al., 2016; McKenzie et al., 2015). NE-Q and NE-HA failed to produce any perceptible changes on the membrane (score < 0.9). Membrane treatment with NE-CET resulted in hyperemia and several small points of hemorrhage, which are marked with black arrows in **Figure 2**, resulting in an irritation score of 1.2 (slightly irritating).

Because NE-CET displayed a higher irritation score compared to the other nanoemulsions, and its zeta potential decreased with time (which is a possible indicative of lower stability) we opted to exclude NE-CET from further studies, and focused on the comparison of a cationic (NE-Q) and an anionic (NE-HA) nanoemulsion.

2.3. Morphological characterization: analysis of NE-Q and NE-HA using transmission electron microscopy demonstrated the presence of fairly spherical electron-dense structures with a diameter of less than 100 nm (between 40 and 70 nm, **Figure 3A-B**). These results are consistent with light scattering findings, which demonstrated droplets with average diameters of 58.4 and 74.1 nm for NE-HA and NE-Q, respectively (**Figure 1**, 0 days).

2.4. DSC analysis: this experiment was conducted to determine the glass transition temperature (Tg') and gain more information regarding the interactions occurring within the nanoemulsion upon addition of hyaluronic acid and chitosan. Addition of hyaluronic acid altered several parameters of the DSC curve compared to NE without polymers. In the heating cycle, addition of hyaluronic acid increased Tg' from -45 to -36 °C, the melting peak temperature (T_{peak}) from -0.8 to + 1.4 °C, and enthalpy of fusion (ΔH_{fus}) from 214.7 to 243.0 J/g (**Table 4, Supplementary Figure 3**); increases in the enthalpy of crystallization (ΔH_{crys}) and exotermic freezing peak temperature ($T_{peak\text{-}crys}$) were also observed in the freezing cycle. The opposite effect was observed when chitosan was included: Tg' decreased to -60°C and ΔH_{fus} to 179.8 J/g. These results suggest

that the polymers affect differently the mobility of water at the vicinity of interfaces, leading to opposing effects on ice formation and vitrification (Droste and Dibenedetto, 1969; Talik and Hubicka, 2018). It is also noteworthy to mention that DSC curves of NE, NE-Q and NE-HA showed a single and narrow exothermic event upon cooling, which is typical for monodispersed O/W systems and congruent with the observed particle size distribution results (Clausse, 1998).

2.5. Rheological behavior: both nanoemulsions displayed Newtonian behavior independent on the type of bioadhesive polymer as demonstrated by linear relationships between the rate of shear and shear stress (**Supplementary Figure 4**), which resulted in flow index values in the range 0.95-0.99. The viscosity, calculated as the average of viscosity at individual values of shear rate, was 0.014 ± 0.002 Pa.s for NE-Q and 0.008 ± 0.001 Pa.s for NE-HA demonstrating that, even though the rheological behavior was similar, addition of chitosan promoted an 1.5-fold increase in viscosity compared to hyaluronic acid.

2.6. In vitro bioadhesive properties: bioadhesive characteristics are important when prolonged residence time is intended. Bioadhesive properties were evaluated by means of a tensile test, in which the maximum force to detach the nanoemulsions from the subcutaneous tissue of skin sections was determined. The force necessary to detach NE-Q and NE-HA was ~1.9- and 1.7-fold higher, respectively, than that necessary to detach water ($p < 0.05$), suggesting a stronger interaction between these formulations and the tissue (**Figure 3C**). The detachment forces for NE-Q and NE-HA were not significantly different.

3. In vivo intraductal administration, mammary tissue targeting and histological assessment

Having demonstrated that NE-HA and NE-Q displayed *in vitro* bioadhesive properties and low irritation potential, their *in vivo* ability to provide localization of Alexa fluor and induce histological changes in the mammary tissue was compared.

Figure 4A depicts representative images of animals subjected to systemic or intraductal administration of unloaded nanoemulsions, Alexa fluor-loaded NE-Q and NE-HA or Alexa fluor solution. To ensure that fluorescence was related to the presence of Alexa fluor in the tissue, unloaded nanoemulsions were administered, and no fluorescence was detected (treatment with NE-HA is depicted, however, the same results were obtained for NE-Q).

Intraductal administration of Alexa Fluor solution led to fluorescent staining of the mammary tissue at the day of the injection, but it disappeared within 24 h. Compared to the solution, administration of Alexa Fluor-loaded nanoemulsions resulted in stronger fluorescent staining of the mammary tissue up to 120 h. On the other hand, i.p. administration resulted in fluorescent staining mainly in the abdominal cavity, which mostly disappeared after 24 h, demonstrating the advantage of intraductal over systemic administration for mammary tissue targeting.

These results can be better visualized in **Figure 4B**, which depicts a quantitative comparison of the fluorescent staining in multiple animals subjected to the different treatments. NE-Q and NE-HA administration resulted in comparable fluorescence intensity in the mammary tissue and decay along 120 h, suggesting that tissue residence is not dependent on the type of bioadhesive polymer and nanoemulsion charge. The nanoemulsion-mediated staining was stronger at all time points assessed compared to Alexa fluor solution, suggesting that, even though solution administration allowed mammary tissue localization, it resulted in a fast elimination of the fluorescent compound.

Representative histological pictures of the mammary tissue of untreated (control) or animals treated with saline, unloaded NE-Q or NE-HA are depicted in **Figure 5**. As previously

570 described, untreated animals display ducts formed by a layer of cuboidal epithelial cells
571 embedded in stroma and surrounded by adipose tissue, often referred to as the fat pad (Masso-
572 Welch et al., 2000). The mammary tissue of animals treated with saline, NE-Q and NE-HA
573 displayed similar architecture compared to untreated animals. The absence of histological
574 alterations (such as edema, infiltration of inflammatory cells and thickening of the ductal layer
575 and lobular units) suggests tissue integrity.
576
577 ***4. Stability and drug release***
578 Since NE-HA and NE-Q provided similar *in vivo* retention of Alexa fluor and induced no
579 perceptible histological alterations in the mammary tissue, piplartine was incorporated in these
580 formulations for comparisons of drug release and stability.
581 The maximum amount of piplartine that could be encapsulated in the nanoemulsions was
582 1% (w/w); larger amounts (2%) could be initially dissolved, but precipitation was observed
583 within 24 h. At this concentration, piplartine incorporation did not significantly ($p > 0.05$) affect
584 size, PDI or zeta potential (**Figure 6 A-C**, time=0 days, **Supplementary Table 1**).
585 Changes in the physicochemical characteristics of piplartine-loaded NE-Q and NE-HA
586 were assessed for 60 days. No alterations, such as creaming, formation of aggregates or phase
587 separation, were observed macroscopically or under a light microscope, but NE-Q size increased
588 in a significant manner ($p < 0.05$) after 45 and 60 days (**Figure 6A**). Interestingly, this change
589 was preceded by an increase in PDI at 30 days (**Figure 6B**). No significant changes were
590 observed on zeta potential (**Figure 6C**).
591 Piplartine content after nanoemulsion sonication was ~100% of its initial content before
592 sonication. As can be observed in **Figure 6D**, it remained between 96 and 108% of the initial
593 content for 60 days, suggesting that piplartine is stable in both NE-Q and NE-HA.

Considering drug lipophilicity (logP = 2.37) (Lee et al., 2018), we anticipated the possibility of piplartine remaining associated with the formulation and having its cellular cytotoxicity decreased. To assess drug release, *in vitro* studies were performed. Very similar amounts of piplartine were released comparing the two nanoemulsions, and at the longest time point studied (16 h), 29 – 34% of piplartine was released from NE-Q and NE-HA (**Figure 6E**). Similar piplartine amounts were observed in the receptor phase after 6 h when a drug in solution was employed, suggesting that drug diffusion across the membrane was not a rate-limiting step in the release process. During the 16 h period, linear relationships were obtained when cumulative drug release was plotted as a function of time ($r > 0.99$), suggesting zero-order kinetics, which is in accordance with other studies (Migotto et al., 2018; Tayel et al., 2013; Zhang et al., 2013).

DISCUSSION

The first goal of this study was to optimize the composition and production parameters of nanoemulsions for intraductal drug delivery. Although nanoemulsions are most often formed by synthetic surfactants such as polysorbates, the desire to obtain formulations with improved biocompatibility and free of synthetic ingredients has prompted studies for optimization using phospholipids (Komaiko et al., 2016). Thus, we started this study assessing the possibility to produce nanoemulsions using soy PC as sole surfactant. However, we did not succeed, and a possible reason was the low phospholipid-oil phase ratio employed; ratios higher than 1:1 seem to be necessary to reduce droplet size and form nanoemulsions (Komaiko et al., 2016). Combining PC with polysorbate 80 and glycerol gave rise to nanoemulsions, which is consistent with their ability to destabilize liquid crystalline phases and lamellas preferentially formed by PC, favoring nano and microemulsions (Hoeller et al., 2009; Lopes et al., 2006; Patel et al., 2006). Besides polysorbate and glycerol, other surfactants employed for nanoemulsion stabilization include

619 lauric arginate, deoxycholic acid and Cremophor EL (Ma et al., 2016; Musa et al., 2013; Vyas et
620 al., 2008).

621 The second factor assessed was aqueous phase temperature. It is well known that
622 temperature is important for emulsification, and aqueous and oil phase heating at 40–80°C aids
623 formation of coarse emulsions (Floyd, 1999). However, the effect of aqueous phase temperature
624 on nanoemulsion production has been less explored. An *et al.* (2014) reported droplet size
625 reduction when the aqueous phase temperature increased from 25 to 50 °C, an effect attributed to
626 viscosity reduction and increased surfactant aqueous solubility (An et al., 2014; Anton and
627 Vandamme, 2009; Lefebvre et al., 2017). In the present study, the nanoemulsion diameter
628 obtained upon 20 min of sonication was similar regardless of the temperature of the aqueous
629 phase, but this diameter was reached with a shorter sonication period (5-10 min) upon aqueous
630 phase heating. Considering that unanticipated sample responses to the generated heat and
631 titanium contamination from the probe increase with sonication time (Betts et al., 2013), aqueous
632 phase heating and sonication time reduction can improve sample quality.

633 Subsequently, the influence of two other surfactants on nanoemulsion characteristics was
634 assessed. Poloxamer 407 produces temperature-sensitive gels at concentrations varying from
635 1.5% to 30% (Giuliano et al., 2018), and although a concentration below this range was
636 employed, formulation gelling occurred after 2 months, leading to its exclusion from
637 nanoemulsion composition. Gelling might result from the interference of formulation components
638 on hydration of the PEO and PPO blocks, and consequently, on micellization as demonstrated
639 previously for salts and co-solvents (Bodratti and Alexandridis, 2018). Chitosan, for example, has
640 been described to reduce poloxamer critical micellization temperature (Ur-Rehman et al., 2011).
641 At 0.5%, cetylpyridinium chloride imparted a positive charge to the nanoemulsions but also
642 increased its irritation potential. This was not surprising as this concentration is higher than the
643 range used in products for oral hygiene (0.02-0.2%) and for nanocrystals aimed for safe ocular

644 drug delivery (0.01%) (Lin and Hemming, 1996; Romero et al., 2016). The risk of increasing
645 irritation to the mammary tissue led us to exclude NE-CET from further studies.

646 Having defined the process parameters and composition of nanoemulsions, the influence
647 of chitosan and hyaluronic acid on the characteristics and properties of nanoemulsions were
648 compared. Formation of nanocarriers composed of phospholipids and charged polysaccharides
649 involve attractive interactions of the polar headgroup of the amphiphilic lipid with the
650 polysaccharide, while its hydrophobic portions interact with the oil phase component (in this
651 case, tricaprylin) (Gerelli et al., 2008). Previous studies suggested formation of particles with a
652 polymer shell surrounding an oily core and/or multilayered structures with alternating layers of
653 phospholipids and hydrated polymer (Gerelli et al., 2008).

654 DSC analysis revealed that chitosan and hyaluronic acid had opposite effects on Tg'.
655 Defined as the temperature at which an amorphous material changes from a glassy, solid-like
656 state to a rubbery state upon heating, Tg' is important to predict interactions within the sample
657 and stability (Droste and Dibenedetto, 1969). The decrease in Tg' observed upon chitosan
658 addition suggests a stronger interaction of this polysaccharide with the aqueous phase compared
659 to hyaluronic acid, favoring the existence of the non-freezable water. Further findings also
660 support this fact: the high degree of supercooling of the NE-Q sample, represented by the lowest
661 $T_{peak\text{-}cryst}$ value, and a decrease in the enthalpy of fusion of ice when compared to NE (without
662 bioadhesive polymers) or NE-HA. The first indicates a slow nucleation and ice growth (Williams
663 and Polli, 1988). The second is an evidence of a proportional decrease of unbound water, i.e.
664 freezable water; by dividing ΔH_{fus} of each sample by the heat of fusion of pure ice (330 J/g)
665 (Samouillan et al., 2012), we estimated approximately 73.6% and 65.1% of freezable water
666 content for NE-HA and NE, respectively, against only 54.5% for NE-Q. This effect might result
667 from a chitosan-induced increase in viscosity, similarly to the effect previously described for β-
668 casein (Maher et al., 2011), and is in accordance with our rheology findings. In spite of the

669 viscosity difference, the *in vitro* bioadhesive property of the two nanoemulsions was similar,
670 suggesting that the type and charge of the polymer may not influence local residence.

671 Although bioadhesion can be influenced by viscosity, its mechanisms are complex and
672 variable, involving multiple stages that include contact, hydration, wetting and spreading, as well
673 as a consolidation stage, in which penetration of the polymer chains into the mucus layer and
674 bonding occurs (Machado et al., 2017). Positively charged chitosan are capable of forming
675 polyelectrolyte complexes with negatively charged mucus components, whereas formation of
676 hydrogen bonds has been suggested to contribute to bioadhesion of negatively charged hyaluronic
677 acid (Oh et al., 2015). Compared to other formulations described in the literature, our
678 nanoemulsions did not exhibit strong bioadhesiveness, which was expected based on their low
679 viscosity, high aqueous content and low concentration of the bioadhesive components (Bento da
680 Silva et al., 2017; Jin et al., 2016); however, compared to simple aqueous solutions, the higher
681 detachment force of NE-Q and NE-HA may be useful to increase residence time in the mammary
682 tissue.

683 *In vivo* results confirmed the ability of the nanoemulsions to extend retention compared to
684 a simple solution, and reinforced the similar profile of NE-Q and NE-HA. The rapid tissue
685 removal of Alexa fluor when administered intraductally as a solution is consistent with the small
686 $t_{1/2}$ (approximately 15 min) previously described for fluorescein administered through the same
687 route as a solution (Singh et al., 2012). The fact that NEQ and NEHA depicted similar mammary
688 tissue retention corroborates *in vitro* bioadhesion observations, and suggests that the *in vitro*
689 assay is useful for the screening of intraductal formulations. The type of polymer did not
690 influence the occurrence of irritation to the site of administration, as none of the nanoemulsions
691 promoted perceptible changes on the vasculature of CAM membranes or histological changes in
692 the mammary tissue. In addition to demonstrating that the nanoemulsions do not cause any
693 histological changes in the mammary tissue, this study provides further evidence of the

applicability of HET-CAM as an alternative method to assess irritation at the administration site (Eichenbaum et al., 2013).

Piplartine was stable in both nanoemulsions for 60 days. However, although NE-Q did not show macroscopic signs of coalescence, precipitation or phase separation, particle size increased at 45 and 60 days. This increase might impact drug release and bioavailability as suggested by previous studies that assessed the influence of size on drug transport across barriers; diazepam for example, had its skin penetration increased upon droplet size reduction from the macro to the nanorange (100-300 nm) (Schwarz et al., 1995; Zhou et al., 2009). Future studies will compare the cytotoxicity and efficacy of these nanoemulsions in breast cancer models.

CONCLUSION

The impact of formulation components and production parameters on the obtainment of nanoemulsions suitable for intraductal administration of piplartine were assessed. Combination of PC, polysorbate 80 and glycerol as surfactant blend mixed at a 1:1 ratio with the oil phase resulted in nanoemulsions with $d < 100$ nm. Aqueous phase content and temperature played significant roles, with heating at 50°C enabling sonication time reduction. Bioadhesive properties of NE-Q and NE-HA were similar as demonstrated *in vitro* by a similar detachment force from the tissue, and *in vivo* by prolonging mammary tissue retention without causing tissue damage, suggesting that the type and charge of bioadhesive polymer does not largely influence these properties. These results demonstrate the potential of both NE-Q and NE-HA for intraductal administration, but because the droplet size of piplartine-loaded NE-HA was maintained at a similar range for longer periods of time, this nanoemulsion might be more promising.

ACKNOWLEDGEMENTS

The authors would like to thank Dr. Catherine Dreiza (Estrella Mountain Community College, Phoenix, AZ) for language revision. This study was supported by São Paulo Research Foundation (FAPESP, grant# 2013/16617-7, 2018/03418-0 and 2018/13877-1) and National Council of Technological and Scientific Development (CNPq, grant# 443549/2014-1). Fellowships from CNPQ (L.V. Costa-Lotufo), CAPES (finance code 001) and FAPESP (2017/04174-4, 2017/23213-0, 2017/19059-6, 2018/18813-1) are greatly appreciated. Bioimaging analysis was conducted at the CEFAP core facility (Institute of Biomedical Sciences, University of São Paulo). This study was registered at SisGen under number A90EE5B.

REFERENCES

2007. Hen's egg test on the chorioallanthoic membrane (HET-CAM); INVITTOX n. 96.

Akima, K., Ito, H., Iwata, Y., Matsuo, K., Watari, N., Yanagi, M., Hagi, H., Oshima, K., Yagita, A., Atomi, Y., Tatekawa, I., 1996. Evaluation of antitumor activities of hyaluronate binding antitumor drugs: synthesis, characterization and antitumor activity. J Drug Target 4, 1-8.

An, Y., Yan, X., Li, B., Li, Y., 2014. Microencapsulation of capsanthin by self-emulsifying nanoemulsions and stability evaluation. European Food Research and Technology 239, 1077-1085.

Anton, N., Vandamme, T.F., 2009. The universality of low-energy nano-emulsification. Int J Pharm 377, 142-147.

Benson, J.R., Jatoi, I., Toi, M., 2016. Treatment of low-risk ductal carcinoma in situ: is nothing better than something? Lancet Oncol 17, e442-e451.

Bento da Silva, P., Fioramonti Calixto, G.M., Oshiro Júnior, J.A., Bombardelli, R.L.Á., Fonseca-Santos, B., Rodero, C.F., Chorilli, M., 2017. Structural features and the anti-inflammatory effect of green tea extract-loaded liquid crystalline systems intended for skin delivery. Polymers 9, 30.

Betts, J.N., Johnson, M.G., Rygiewicz, P.T., King, G.A., Andersen, C.P., 2013. Potential for metal contamination by direct sonication of nanoparticle suspensions. Environmental toxicology and chemistry 32, 889-893.

Bezerra, D.P., de Castro, F.O., Alves, A.P., Pessoa, C., de Moraes, M.O., Silveira, E.R., Lima, M.A., Elmiro, F.J., de Alencar, N.M., Mesquita, R.O., Lima, M.W., Costa-Lotufo, L.V., 2008a. In vitro and in vivo antitumor effect of 5-FU combined with piplartine and piperine. Journal of applied toxicology : JAT 28, 156-163.

Bezerra, D.P., Militao, G.C., de Castro, F.O., Pessoa, C., de Moraes, M.O., Silveira, E.R., Lima, M.A., Elmiro, F.J., Costa-Lotufo, L.V., 2007. Piplartine induces inhibition of leukemia cell proliferation triggering both apoptosis and necrosis pathways. Toxicol In Vitro 21, 1-8.

Bezerra, D.P., Moura, D.J., Rosa, R.M., de Vasconcellos, M.C., e Silva, A.C., de Moraes, M.O., Silveira, E.R., Lima, M.A., Henriques, J.A., Costa-Lotufo, L.V., Saffi, J., 2008b. Evaluation of the genotoxicity of piplartine, an alkamide of Piper tuberculatum, in yeast and mammalian V79 cells. Mutat Res 652, 164-174.

Bezerra, D.P., Pessoa, C., de Moraes, M.O., Saker-Neto, N., Silveira, E.R., Costa-Lotufo, L.V., 2013. Overview of the therapeutic potential of piplartine (piperlongumine). Eur J Pharm Sci 48, 453-463.
Bodratti, A.M., Alexandridis, P., 2018. Formulation of Poloxamers for Drug Delivery. Journal of functional biomaterials 9.
Brewster, M.E., Vandecruys, R., Verreck, G., Peeters, J., 2008. Supersaturating drug delivery systems: effect of hydrophilic cyclodextrins and other excipients on the formation and stabilization of supersaturated drug solutions. Pharmazie 63, 217-220.
Campbell, M.J., Baehner, F., O'Meara, T., Ojukwu, E., Han, B., Mukhtar, R., Tandon, V., Endicott, M., Zhu, Z., Wong, J., Krings, G., Au, A., Gray, J.W., Esserman, L., 2017. Characterizing the immune microenvironment in high-risk ductal carcinoma in situ of the breast. Breast Cancer Res Treat 161, 17-28.
Carvalho, V.F., de Lemos, D.P., Vieira, C.S., Migotto, A., Lopes, L.B., 2017a. Potential of Non-aqueous Microemulsions to Improve the Delivery of Lipophilic Drugs to the Skin. AAPS PharmSciTech 18, 1739-1749.
Carvalho, V.F.M., Giacone, D.V., Costa-Lotufo, L.V., Silveira, E.R., Lopes, L.B., 2019. Development of a method for quantitative determination of the cytotoxic agent piplartine (piperlongumine) in multiple skin layers. Biomed Chromatogr 33, e4386.
Carvalho, V.F.M., Migotto, A., Giacone, D.V., de Lemos, D.P., Zanoni, T.B., Maria-Engler, S.S., Costa-Lotufo, L.V., Lopes, L.B., 2017b. Co-encapsulation of paclitaxel and C6 ceramide in tributyrin-containing nanocarriers improve co-localization in the skin and potentiate cytotoxic effects in 2D and 3D models. Eur J Pharm Sci 109, 131-143.
Chang, C.M., Bodmeier, R., 1997. Swelling of and drug release from monoglyceride-based drug delivery systems. J Pharm Sci 86, 747-752.
Chun, Y.S., Bisht, S., Chenna, V., Pramanik, D., Yoshida, T., Hong, S.M., de Wilde, R.F., Zhang, Z., Huso, D.L., Zhao, M., Rudek, M.A., Stearns, V., Maitra, A., Sukumar, S., 2012. Intraductal administration of a polymeric nanoparticle formulation of curcumin (NanoCurc) significantly attenuates incidence of mammary tumors in a rodent chemical carcinogenesis model: Implications for breast cancer chemoprevention in at-risk populations. Carcinogenesis 33, 2242-2249.
Cichewicz, A., Pacleb, C., Connors, A., Hass, M.A., Lopes, L.B., 2013. Cutaneous delivery of alpha-tocopherol and lipoic acid using microemulsions: influence of composition and charge. J Pharm Pharmacol 65, 817-826.
Clausse, D., 1998. Thermal behaviour of emulsions studied by differential scanning calorimetry. Journal of Thermal Analysis and Calorimetry 51, 191-201.
Contri, R.V., Fiel, L.A., Alnasif, N., Pohlmann, A.R., Guterres, S.S., Schafer-Korting, M., 2016. Skin penetration and dermal tolerability of acrylic nanocapsules: Influence of the surface charge and a chitosan gel used as vehicle. Int J Pharm 507, 12-20.
Danaei, M., Dehghankhold, M., Ataei, S., Hasanzadeh Davarani, F., Javanmard, R., Dokhani, A., Khorasani, S., Mozafari, M.R., 2018. Impact of Particle Size and Polydispersity Index on the Clinical Applications of Lipidic Nanocarrier Systems. Pharmaceutics 10.
de Groot, J.S., Moelans, C.B., Elias, S.G., Jo Fackler, M., van Domselaar, R., Suijkerbuijk, K.P., Witkamp, A.J., Sukumar, S., van Diest, P.J., van der Wall, E., 2016. DNA promoter hypermethylation in nipple fluid: a potential tool for early breast cancer detection. Oncotarget 7, 24778-24791.
Droste, D.H., Dibenedetto, A.T., 1969. The glass transition temperature of filled polymers and its effect on their physical properties. Journal of Applied Polymer Science 13, 2149-2168.
Eichenbaum, G., Zhou, J., De Smedt, A., De Jonghe, S., Looszova, A., Arien, T., Van Goethem, F., Vervoort, I., Shukla, U., Lammens, L., 2013. Methods to evaluate and improve the injection site tolerability of intravenous formulations prior to first-in-human testing. J Pharmacol Toxicol Methods 68, 394-406.
Fallowfield, L., Francis, A., 2016. Overtreatment of Low-Grade Ductal Carcinoma In Situ. JAMA oncology 2, 382-383.
Fangueiro, J.F., Calpena, A.C., Clares, B., Andreani, T., Egea, M.A., Veiga, F.J., Garcia, M.L., Silva, A.M., Souto, E.B., 2016. Biopharmaceutical evaluation of epigallocatechin gallate-loaded cationic lipid nanoparticles (EGCG-LNs): In vivo, in vitro and ex vivo studies. Int J Pharm 502, 161-169.

809 Ferris-James, D.M., Iuanow, E., Mehta, T.S., Shaheen, R.M., Slanetz, P.J., 2012. Imaging approaches to
810 diagnosis and management of common ductal abnormalities. Radiographics : a review publication of the
811 Radiological Society of North America, Inc 32, 1009-1030.
812 Floyd, A.G., 1999. Top ten considerations in the development of parenteral emulsions. Pharmaceutical
813 science & technology today 4, 134-143.
814 Fofaria, N.M., Qhattal, H.S., Liu, X., Srivastava, S.K., 2016. Nanoemulsion formulations for anti-cancer
815 agent piplartine--Characterization, toxicological, pharmacokinetics and efficacy studies. Int J Pharm 498,
816 12-22.
817 Gerelli, Y., Barbieri, S., Di Bari, M.T., Deriu, A., Cantù, L., Brocca, P., Sonvico, F., Colombo, P., May, R.,
818 Motta, S., 2008. Structure of Self-Organized Multilayer Nanoparticles for Drug Delivery. Langmuir 24,
819 11378-11384.
820 Giuliano, E., Paolino, D., Fresta, M., Cosco, D., 2018. Mucosal Applications of Poloxamer 407-Based
821 Hydrogels: An Overview. Pharmaceutics 10.
822 Groen, E.J., Elshof, L.E., Visser, L.L., Rutgers, E.J., Winter-Warnars, H.A., Lips, E.H., Wesseling, J., 2017.
823 Finding the balance between over- and under-treatment of ductal carcinoma in situ (DCIS). Breast
824 (Edinburgh, Scotland) 31, 274-283.
825 Gu, Z., Al-Zubaydi, F., Adler, D., Li, S., Johnson, S., Prasad, P., Holloway, J., Szekely, Z., Love, S., Gao, D.,
826 Sinko, P.J., 2018. Evaluation of intraductal delivery of poly(ethylene glycol)-doxorubicin conjugate
827 nanocarriers for the treatment of ductal carcinoma in situ (DCIS)-like lesions in rats. Journal of
828 interdisciplinary nanomedicine 3, 146-159.
829 Guter, M., Breunig, M., 2017. Hyaluronan as a promising excipient for ocular drug delivery. Eur J Pharm
830 Biopharm 113, 34-49.
831 Hoeller, S., Sperger, A., Valenta, C., 2009. Lecithin based nanoemulsions: A comparative study of the
832 influence of non-ionic surfactants and the cationic phytosphingosine on physicochemical behaviour and
833 skin permeation. Int J Pharm 370, 181-186.
834 Hosmer, J.M., Steiner, A.A., Lopes, L.B., 2013. Lamellar liquid crystalline phases for cutaneous delivery of
835 Paclitaxel: impact of the monoglyceride. Pharm Res 30, 694-706.
836 Jin, S.G., Yousaf, A.M., Kim, K.S., Kim, D.W., Kim, D.S., Kim, J.K., Yong, C.S., Youn, Y.S., Kim, J.O., Choi,
837 H.G., 2016. Influence of hydrophilic polymers on functional properties and wound healing efficacy of
838 hydrocolloid based wound dressings. Int J Pharm 501, 160-166.
839 Komaiko, J., Sastrosubroto, A., McClements, D.J., 2016. Encapsulation of omega-3 fatty acids in
840 nanoemulsion-based delivery systems fabricated from natural emulsifiers: Sunflower phospholipids.
841 Food chemistry 203, 331-339.
842 Kong, E.H., Kim, Y.J., Cho, H.J., Yu, S.N., Kim, K.Y., Chang, J.H., Ahn, S.C., 2008. Piplartine induces caspase-
843 mediated apoptosis in PC-3 human prostate cancer cells. Oncol Rep 20, 785-792.
844 Krause, S., Brock, A., Ingber, D.E., 2013. Intraductal injection for localized drug delivery to the mouse
845 mammary gland. J Vis Exp.
846 Land, L.M., Li, P., Bummer, P.M., 2006. Mass transport properties of progesterone and estradiol in model
847 microemulsion formulations. Pharm Res 23, 2482-2490.
848 Lee, H.L., Hwang, S.C., Nah, J.W., Kim, J., Cha, B., Kang, D.H., Jeong, Y.I., 2018. Redox- and pH-Responsive
849 Nanoparticles Release Piperlongumine in a Stimuli-Sensitive Manner to Inhibit Pulmonary Metastasis of
850 Colorectal Carcinoma Cells. J Pharm Sci 107, 2702-2712.
851 Lefebvre, G., Riou, J., Bastiat, G., Roger, E., Frombach, K., Gimel, J.C., Saulnier, P., Calvignac, B., 2017.
852 Spontaneous nano-emulsification: Process optimization and modeling for the prediction of the
853 nanoemulsion's size and polydispersity. Int J Pharm 534, 220-228.
854 Lin, G.H., Hemming, M., 1996. Ocular and dermal irritation studies of some quaternary ammonium
855 compounds. Food Chem Toxicol 34, 177-182.
856 Lopes, L.B., Murphy, N., Nornoo, A., 2009. Enhancement of transdermal delivery of progesterone using
857 medium-chain mono and diglycerides as skin penetration enhancers. Pharm Dev Technol 14, 524-529.
858 Lopes, L.B., Scarpa, M.V., Pereira, N.L., de Oliveira, L.C., Oliveira, A.G., 2006. Interaction of sodium
859 diclofenac with freeze-dried soya phosphatidylcholine and unilamellar liposomes. Rev. Bras. Cienc. Farm.
860 42, 8.

Loureiro, A., Nogueira, E., Azoia, N.G., Sarria, M.P., Abreu, A.S., Shimanovich, U., Rollett, A., Harmark, J., Hebert, H., Guebitz, G., Bernardes, G.J., Preto, A., Gomes, A.C., Cavaco-Paulo, A., 2015. Size controlled protein nanoemulsions for active targeting of folate receptor positive cells. Colloids Surf B Biointerfaces 135, 90-98.

Love, S.M., Zhang, W., Gordon, E.J., Rao, J., Yang, H., Li, J., Zhang, B., Wang, X., Chen, G., Zhang, B., 2013. A feasibility study of the intraductal administration of chemotherapy. Cancer prevention research 6, 51-58.

Luepke, N.P., 1985. Hen's egg chorioallantoic membrane test for irritation potential. Food Chem Toxicol 23, 287-291.

Ma, Q., Davidson, P.M., Zhong, Q., 2016. Nanoemulsions of thymol and eugenol co-emulsified by lauric arginate and lecithin. Food chemistry 206, 167-173.

Machado, R.M., Palmeira-de-Oliveira, A., Martinez-de-Oliveira, J., Palmeira-de-Oliveira, R., 2017. Vaginal semisolid products: Technological performance considering physiologic parameters. Eur J Pharm Sci 109, 556-568.

Maher, P.G., Fenelon, M.A., Zhou, Y., Kamrul Haque, M., Roos, Y.H., 2011. Optimization of β-Casein Stabilized Nanoemulsions Using Experimental Mixture Design. Journal of Food Science 76, C1108-C1117.

Mahoney, M.E., Gordon, E.J., Rao, J.Y., Jin, Y., Hylton, N., Love, S.M., 2013. Intraductal therapy of ductal carcinoma in situ: a presurgery study. Clinical breast cancer 13, 280-286.

Masso-Welch, P.A., Darcy, K.M., Stangle-Castor, N.C., Ip, M.M., 2000. A developmental atlas of rat mammary gland histology. Journal of mammary gland biology and neoplasia 5, 165-185.

Mazzarino, L., Travelet, C., Ortega-Murillo, S., Otsuka, I., Pignot-Paintrand, I., Lemos-Senna, E., Borsali, R., 2012. Elaboration of chitosan-coated nanoparticles loaded with curcumin for mucoadhesive applications. J Colloid Interface Sci 370, 58-66.

McClements, D.J., 2012. Nanoemulsions versus microemulsions: terminology, differences, and similarities. Soft Matter 8, 1719.

McKenzie, B., Kay, G., Matthews, K.H., Knott, R.M., Cairns, D., 2015. The hen's egg chorioallantoic membrane (HET-CAM) test to predict the ophthalmic irritation potential of a cysteamine-containing gel: Quantification using Photoshop(R) and ImageJ. Int J Pharm 490, 1-8.

Mehling, A., Kleber, M., Hensen, H., 2007. Comparative studies on the ocular and dermal irritation potential of surfactants. Food Chem Toxicol 45, 747-758.

Migotto, A., Carvalho, V.F.M., Salata, G.C., da Silva, F.W.M., Yan, C.Y.I., Ishida, K., Costa-Lotufo, L.V., Steiner, A.A., Lopes, L.B., 2018. Multifunctional nanoemulsions for intraductal delivery as a new platform for local treatment of breast cancer. Drug Deliv 25, 654-667.

Mistry, P.H., Mohapatra, S.K., Dash, A.K., 2012. Effect of high-pressure homogenization and stabilizers on the physicochemical properties of curcumin-loaded glycerol monooleate/chitosan nanostructures. Nanomedicine (London, England) 7, 1863-1876.

Mojeiko, G., de Brito, M., Salata, G.C., Lopes, L.B., 2019. Combination of microneedles and microemulsions to increase celecoxib topical delivery for potential application in chemoprevention of breast cancer. Int J Pharm 560, 365-376.

Murata, S., Kominsky, S.L., Vali, M., Zhang, Z., Garrett-Mayer, E., Korz, D., Huso, D., Baker, S.D., Barber, J., Jaffee, E., Reilly, R.T., Sukumar, S., 2006. Ductal access for prevention and therapy of mammary tumors. Cancer Res 66, 638-645.

Musa, S.H., Basri, M., Masoumi, H.R., Karjiban, R.A., Malek, E.A., Basri, H., Shamsuddin, A.F., 2013. Formulation optimization of palm kernel oil esters nanoemulsion-loaded with chloramphenicol suitable for meningitis treatment. Colloids Surf B Biointerfaces 112, 113-119.

Narod, S.A., Iqbal, J., Giannakeas, V., Sopik, V., Sun, P., 2015. Breast Cancer Mortality After a Diagnosis of Ductal Carcinoma In Situ. JAMA oncology 1, 888-896.

Ng, W.Y., Migotto, A., Ferreira, T.S., Lopes, L.B., 2017. Monoolein-alginate beads as a platform to promote adenosine cutaneous localization and wound healing. International journal of biological macromolecules 102, 1104-1111.

Ochoa-Flores, A.A., Hernández-Becerra, J.A., Cavazos-Garduño, A., Soto-Rodríguez, I., Sanchez-Otero, M.G., Vernon-Carter, E.J., García, H.S., 2017. Enhanced Bioavailability of Curcumin Nanoemulsions

913 Stabilized with Phosphatidylcholine Modified with Medium Chain Fatty Acids. Curr Drug Deliv 14, 377-
914 385.
915 Oh, S., Wilcox, M., Pearson, J.P., Borros, S., 2015. Optimal design for studying mucoadhesive polymers
916 interaction with gastric mucin using a quartz crystal microbalance with dissipation (QCM-D): Comparison
917 of two different mucin origins. Eur J Pharm Biopharm 96, 477-483.
918 Okugawa, H., Yamamoto, D., Uemura, Y., Sakaida, N., Tanano, A., Tanaka, K., Kamiyama, Y., 2005. Effect
919 of perductal paclitaxel exposure on the development of MNU-induced mammary carcinoma in female S-
920 D rats. Breast Cancer Res Treat 91, 29-34.
921 Patel, N., Schmid, U., Lawrence, M.J., 2006. Phospholipid-based microemulsions suitable for use in foods.
922 J Agric Food Chem 54, 7817-7824.
923 Pepe, D., McCall, M., Zheng, H., Lopes, L.B., 2013. Protein transduction domain-containing
924 microemulsions as cutaneous delivery systems for an anticancer agent. J Pharm Sci 102, 1476-1487.
925 Pereira, G.G., Detoni, C.B., Balducci, A.G., Rondelli, V., Colombo, P., Guterres, S.S., Sonvico, F., 2016.
926 Hyaluronate nanoparticles included in polymer films for the prolonged release of vitamin E for the
927 management of skin wounds. Eur J Pharm Sci 83, 203-211.
928 Phelps, J., Bentley, M.V., Lopes, L.B., 2011. In situ gelling hexagonal phases for sustained release of an
929 anti-addiction drug. Colloids Surf B Biointerfaces 87, 391-398.
930 Praca, F.S.G., Medina, W.S.G., Eloy, J.O., Petrilli, R., Campos, P.M., Ascenso, A., Bentley, M., 2018.
931 Evaluation of critical parameters for in vitro skin permeation and penetration studies using animal skin
932 models. Eur J Pharm Sci 111, 121-132.
933 Qhattal, H.S., Wang, S., Salihima, T., Srivastava, S.K., Liu, X., 2011. Nanoemulsions of cancer
934 chemopreventive agent benzyl isothiocyanate display enhanced solubility, dissolution, and permeability.
935 J Agric Food Chem 59, 12396-12404.
936 Raj, L., Ide, T., Gurkar, A.U., Foley, M., Schenone, M., Li, X., Tolliday, N.J., Golub, T.R., Carr, S.A., Shamji,
937 A.F., Stern, A.M., Mandinova, A., Schreiber, S.L., Lee, S.W., 2011. Selective killing of cancer cells by a
938 small molecule targeting the stress response to ROS. Nature 475, 231-234.
939 Rege, P.R., Vilivalam, V.D., Collins, C.C., 1998. Development in release testing of topical dosage forms:
940 use of the Enhancer Cell with automated sampling. J Pharm Biomed Anal 17, 1226-1233.
941 Richter, A., Myhre, B., Khanna, S.C., 1969. An automated apparatus for dissolution studies. J Pharm
942 Pharmacol 21, 409-414.
943 Romero, G.B., Keck, C.M., Muller, R.H., Bou-Chacra, N.A., 2016. Development of cationic nanocrystals for
944 ocular delivery. Eur J Pharm Biopharm 107, 215-222.
945 Sagara, Y., Mallory, M.A., Wong, S., Aydogan, F., DeSantis, S., Barry, W.T., Golshan, M., 2015. Survival
946 Benefit of Breast Surgery for Low-Grade Ductal Carcinoma In Situ: A Population-Based Cohort Study.
947 JAMA surgery 150, 739-745.
948 Samouillan, V., Merbahi, N., Yousfi, M., Gardou, J., Delaunay, F., Dandurand, J., Lacabanne, C., 2012.
949 Effect of Low-Temperature Plasma Jet on Thermal Stability and Physical Structure of Type I Collagen. IEEE
950 Transactions on Plasma Science 40, 1688-1695.
951 Schwarz, J., Weisspapir, M., Friedman, D., 1995. Enhanced transdermal delivery of diazepam by
952 submicron emulsion (SME) creams. Pharm Res 12, 687-692.
953 Singh, Y., Gao, D., Gu, Z., Li, S., Rivera, K.A., Stein, S., Love, S., Sinko, P.J., 2012. Influence of molecular size
954 on the retention of polymeric nanocarrier diagnostic agents in breast ducts. Pharm Res 29, 2377-2388.
955 Smart, J.D., 2005. The basics and underlying mechanisms of mucoadhesion. Adv Drug Deliv Rev 57, 1556-
956 1568.
957 Solomon, B., Sahle, F.F., Gebre-Mariam, T., Asres, K., Neubert, R.H., 2012. Microencapsulation of
958 citronella oil for mosquito-repellent application: formulation and in vitro permeation studies. Eur J
959 Pharm Biopharm 80, 61-66.
960 Stearns, V., Mori, T., Jacobs, L.K., Khouri, N.F., Gabrielson, E., Yoshida, T., Kominsky, S.L., Huso, D.L., Jeter,
961 S., Powers, P., Tarpinian, K., Brown, R.J., Lange, J.R., Rudek, M.A., Zhang, Z., Tsangaris, T.N., Sukumar, S.,
962 2011. Preclinical and clinical evaluation of intraductally administered agents in early breast cancer.
963 Science translational medicine 3, 106ra108.

964 Talik, P., Hubicka, U., 2018. The DSC approach to study non-freezing water contents of hydrated
965 hydroxypropylcellulose (HPC). Journal of Thermal Analysis and Calorimetry 132, 445-451.
966 Tayel, S.A., El-Nabarawi, M.A., Tadros, M.I., Abd-Elsalam, W.H., 2013. Promising ion-sensitive in situ
967 ocular nanoemulsion gels of terbinafine hydrochloride: design, in vitro characterization and in vivo
968 estimation of the ocular irritation and drug pharmacokinetics in the aqueous humor of rabbits. Int J
969 Pharm 443, 293-305.
970 Thomas, S., Vieira, C.S., Hass, M.A., Lopes, L.B., 2014. Stability, cutaneous delivery, and antioxidant
971 potential of a lipoic acid and alpha-tocopherol codrug incorporated in microemulsions. J Pharm Sci 103,
972 2530-2538.
973 Tsai, I.L., Lee, F.P., Wu, C.C., Duh, C.Y., Ishikawa, T., Chen, J.J., Chen, Y.C., Seki, H., Chen, I.S., 2005. New
974 cytotoxic cyclobutanoid amides, a new furanoid lignan and anti-platelet aggregation constituents from
975 Piper arborescens. Planta Med 71, 535-542.
976 Ur-Rehman, T., Tavelin, S., Grobner, G., 2011. Chitosan in situ gelation for improved drug loading and
977 retention in poloxamer 407 gels. Int J Pharm 409, 19-29.
978 Vyas, T.K., Shahiwala, A., Amiji, M.M., 2008. Improved oral bioavailability and brain transport of
979 Saquinavir upon administration in novel nanoemulsion formulations. Int J Pharm 347, 93-101.
980 Ward, E.M., DeSantis, C.E., Lin, C.C., Kramer, J.L., Jemal, A., Kohler, B., Brawley, O.W., Gansler, T., 2015.
981 Cancer statistics: Breast cancer in situ. CA: a cancer journal for clinicians 65, 481-495.
982 Williams, N.A., Polli, G.P., 1988. Differential scanning calorimetric studies on frozen cephalosporin
983 solutions. International Journal of Pharmaceutics 44, 205-212.
984 Zhang, B., Love, S.M., Chen, G., Wang, J., Gao, J., Xu, X., Wang, Z., Wang, X., 2014. The safety parameters
985 of the study on intraductal cytotoxic agent delivery to the breast before mastectomy. Chinese journal of
986 cancer research = Chung-kuo yen cheng yen chiu 26, 579-587.
987 Zhang, X., Yi, Y., Qi, J., Lu, Y., Tian, Z., Xie, Y., Yuan, H., Wu, W., 2013. Controlled release of cyclosporine A
988 self-nanoemulsifying systems from osmotic pump tablets: near zero-order release and pharmacokinetics
989 in dogs. Int J Pharm 452, 233-240.
990 Zhou, H., Yue, Y., Liu, G., Li, Y., Zhang, J., Gong, Q., Yan, Z., Duan, M., 2009. Preparation and
991 characterization of a lecithin nanoemulsion as a topical delivery system. Nanoscale research letters 5,
992 224-230.

993

994

995 **Figure captions**

996

997

998 **Figure 1.** Nanoemulsion stability as a function of time, assessed as alterations on size, PDI and
999 zeta potential of NE-Q, NE-HA and NE-CET.

1000

1001 **Figure 2.** Irritation potential of unloaded nanoemulsions evaluated as changes on CAM after
1002 exposure to the nanoemulsions, saline (negative control) or NaOH (0.1 M, positive control) for 5

1003 min. The black arrows depict areas of hemorrhage in the membrane treated with NE-CET. Scale
1004 bar= 1 mm.
1005
1006 **Figure 3.** Characterization of NE-Q and NE-HA morphology and properties. A: transmission
1007 electron microscopy of NE-Q, B: transmission electron microscopy of NE-HA, C: *in vitro*
1008 bioadhesive potential represented by the maximum (peak) force. **$p < 0.01$ compared to water.
1009 Scale bar= 100 nm.
1010
1011 **Figure 4.** *In vivo* mammary tissue targeting and retention of the fluorescent marker Alexa fluor
1012 administered in nanoemulsions or as a solution. A: whole animal images showing fluorescence
1013 staining after intraductal or intraperitoneal (i.p.) administration of the nanoemulsions or control
1014 solutions; B: mammary tissue fluorescence intensity decay as a function of time, N=3-4
1015 animals/group. ** $p < 0.01$ and * $p < 0.05$ compared to Alexa fluor solution, Scale bar= 1 mm.
1016
1017 **Figure 5.** Histological sections of mammary tissue of animals administered with saline, NE-Q
1018 our NE-HA in comparison with untreated animals. The images depict the integrity of ducts and
1019 absence of inflammatory cell infiltrates and edema, bar = 50 μm.
1020
1021 **Figure 6.** Formulation stability and release of piplartine from NE-Q and NE-HA as a function of
1022 time. A-C: changes on size (A), PDI (B) and zeta potential (C) of piplartine-loaded
1023 nanoemulsions; D: changes on piplartine content in the nanoemulsions; E: cumulative piplartine
1024 release from nanoemulsions or a control solution as a function of time.

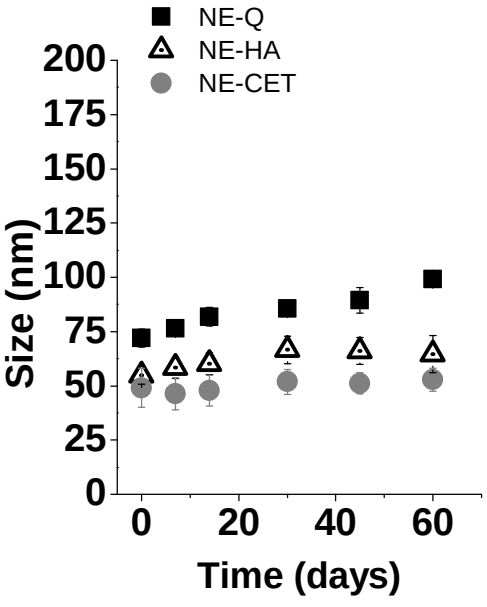
NE-Q
NE-HA
NE-CET
Size (nm)
Time (days)

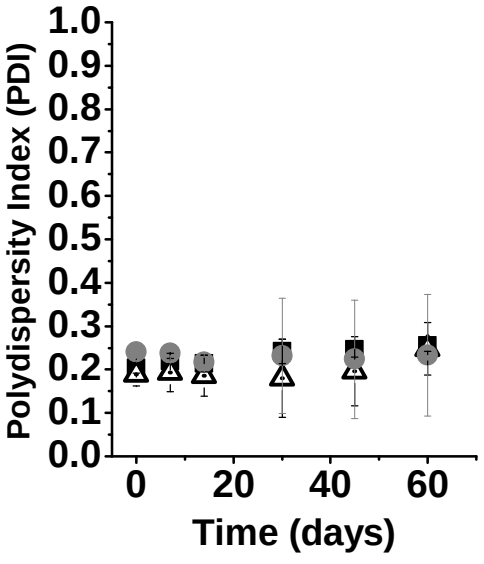
Polydispersity Index (PDI)
Time (days)

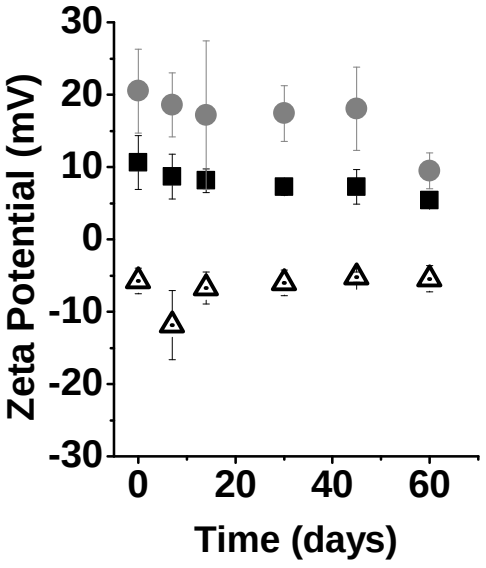
Zeta Potential (mV)
Time (days)

Figure 2

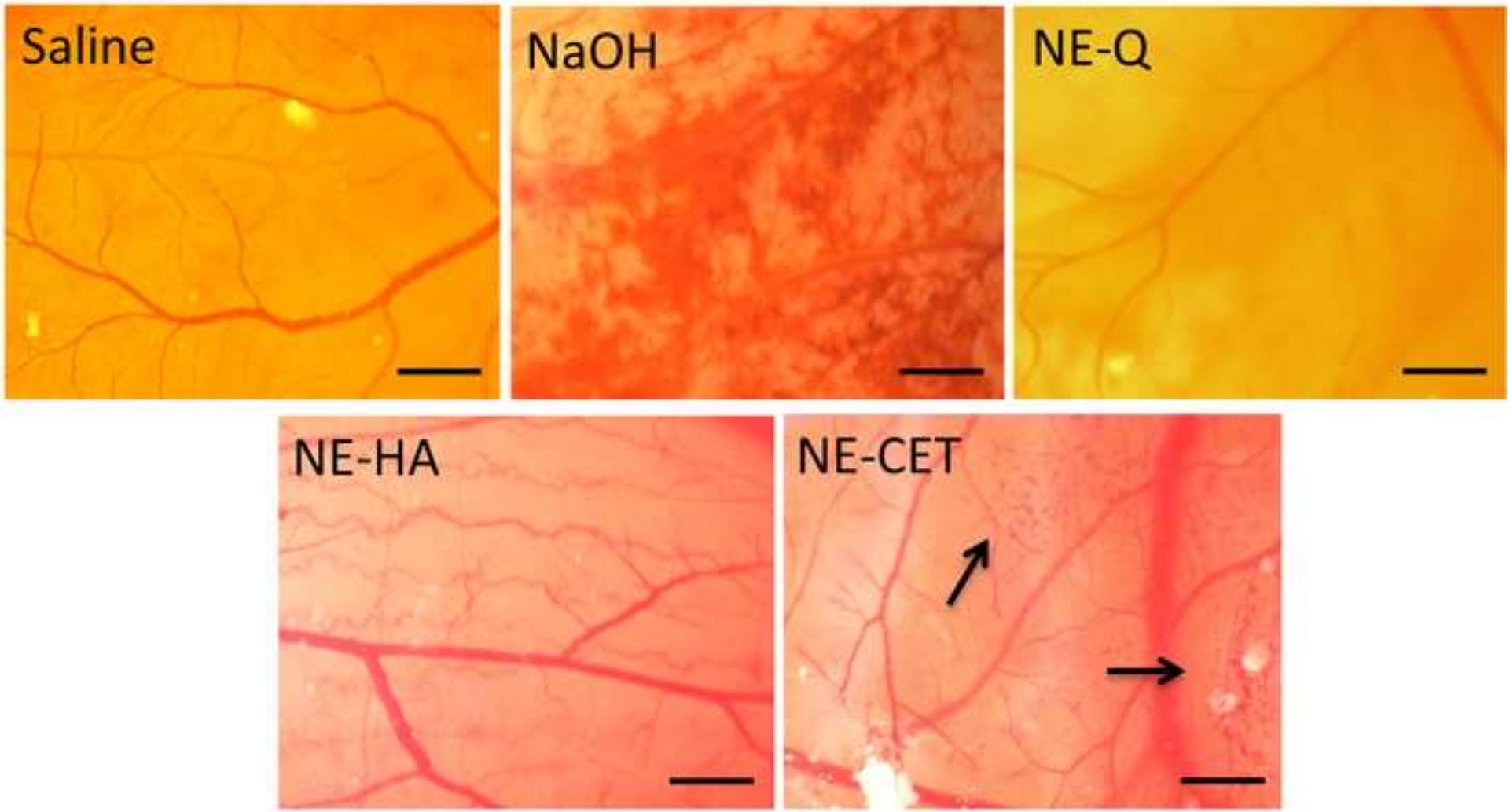

Figure 3

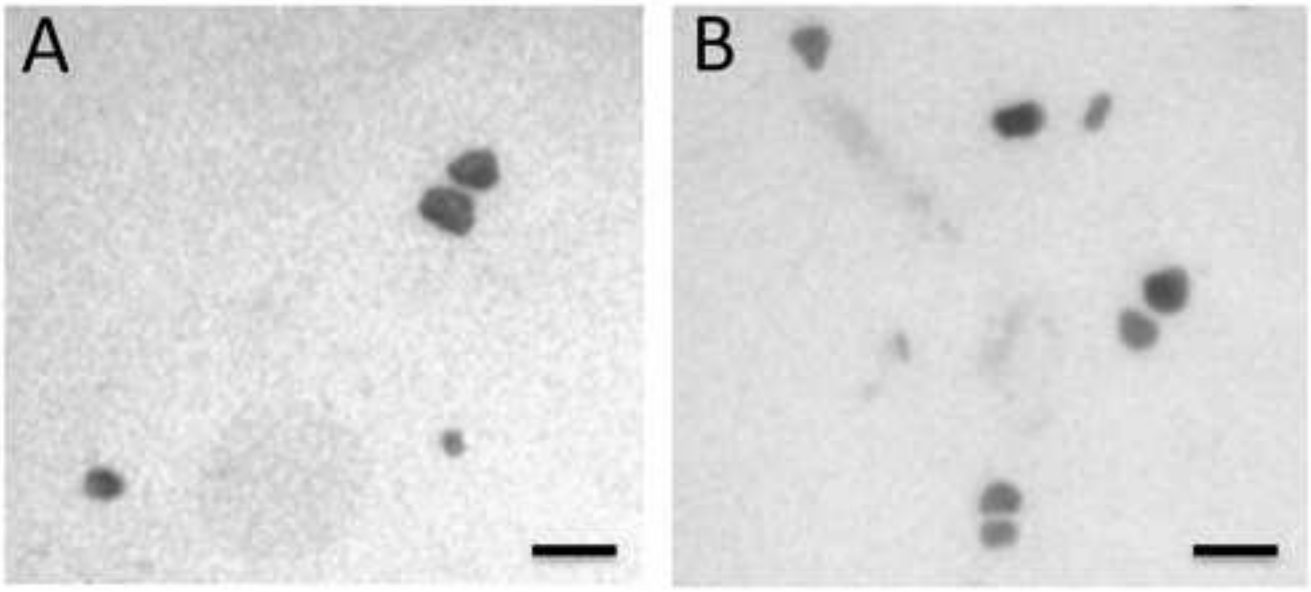
A
B

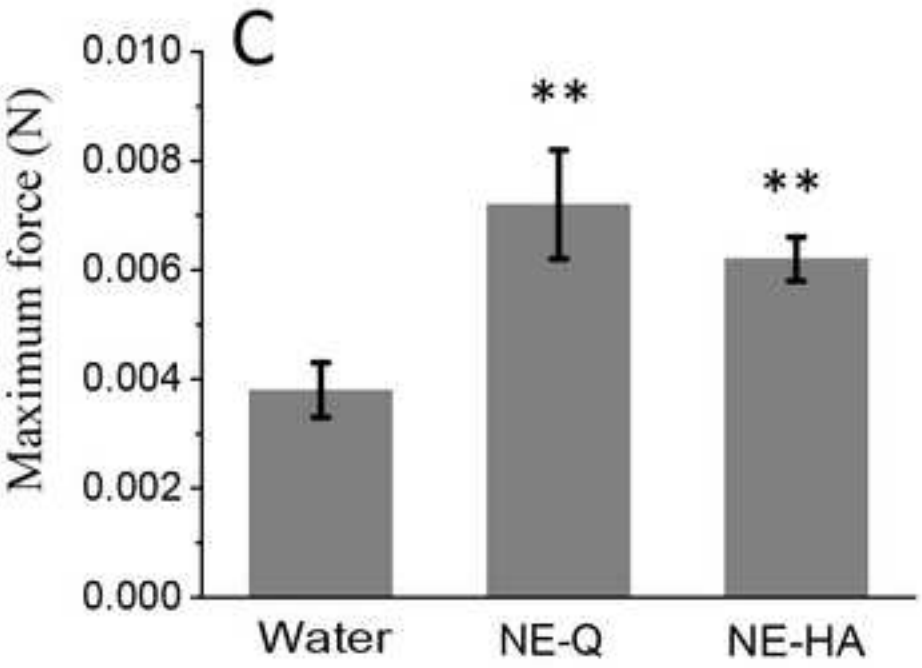
C
Maximum force (N)
0.010
0.008
0.006
0.004
0.002
0.000
**
**
Water
NE-Q
NE-HA

Figure 4

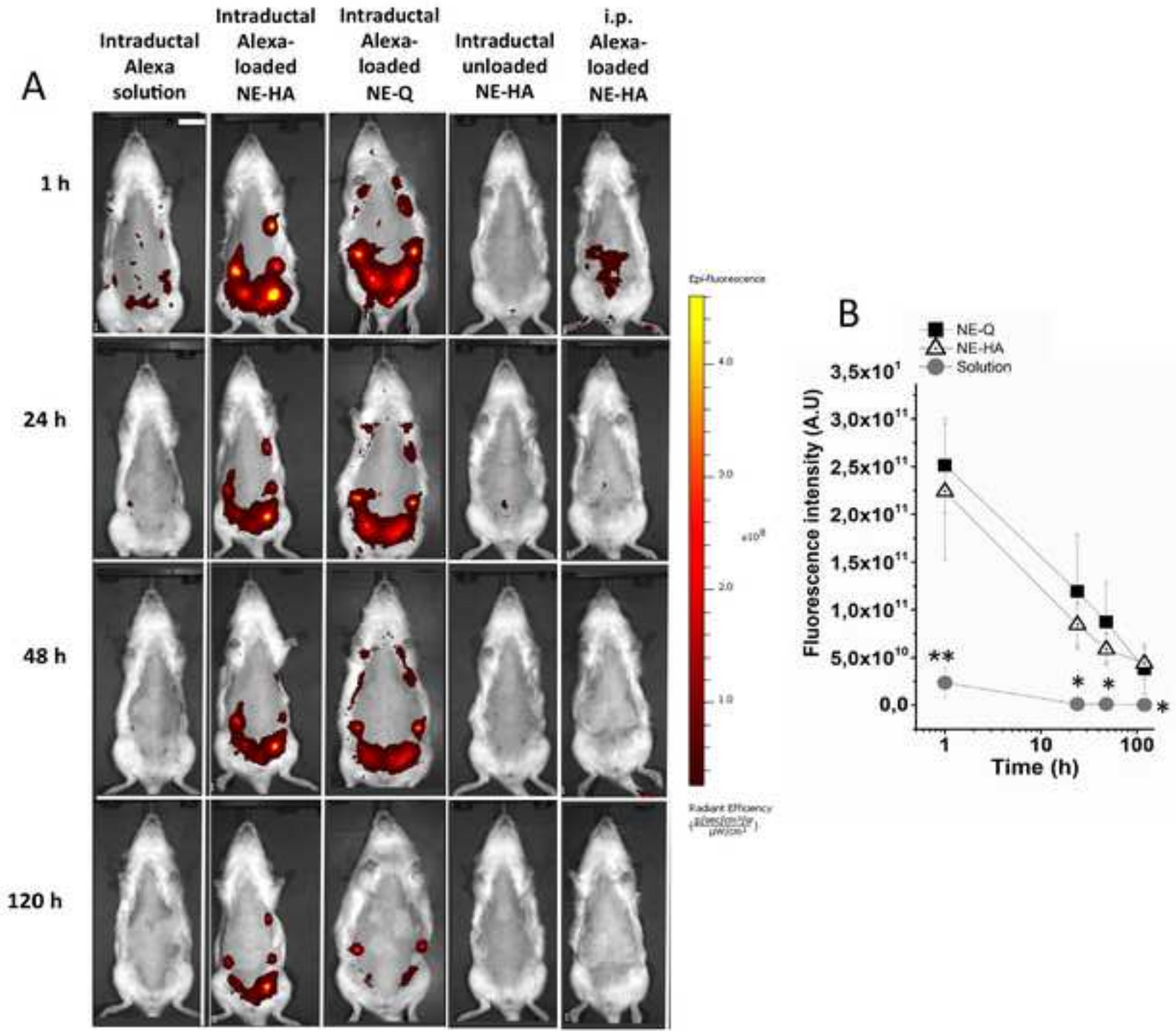
A
Intraductal Alexa solution
Intraductal Alexa-loaded NE-HA
Intraductal Alexa-loaded NE-Q
Intraductal unloaded NE-HA
i.p. Alexa-loaded NE-HA
1 h
24 h
48 h
120 h
Epi-fluorescence
Radiant Efficiency
B
NE-Q
NE-HA
Solution
Fluorescence intensity (A.U)
3,5x10¹¹
3,0x10¹¹
2,5x10¹¹
2,0x10¹¹
1,5x10¹¹
1,0x10¹¹
5,0x10¹⁰
0,0
1
10
100
Time (h)

Figure 5

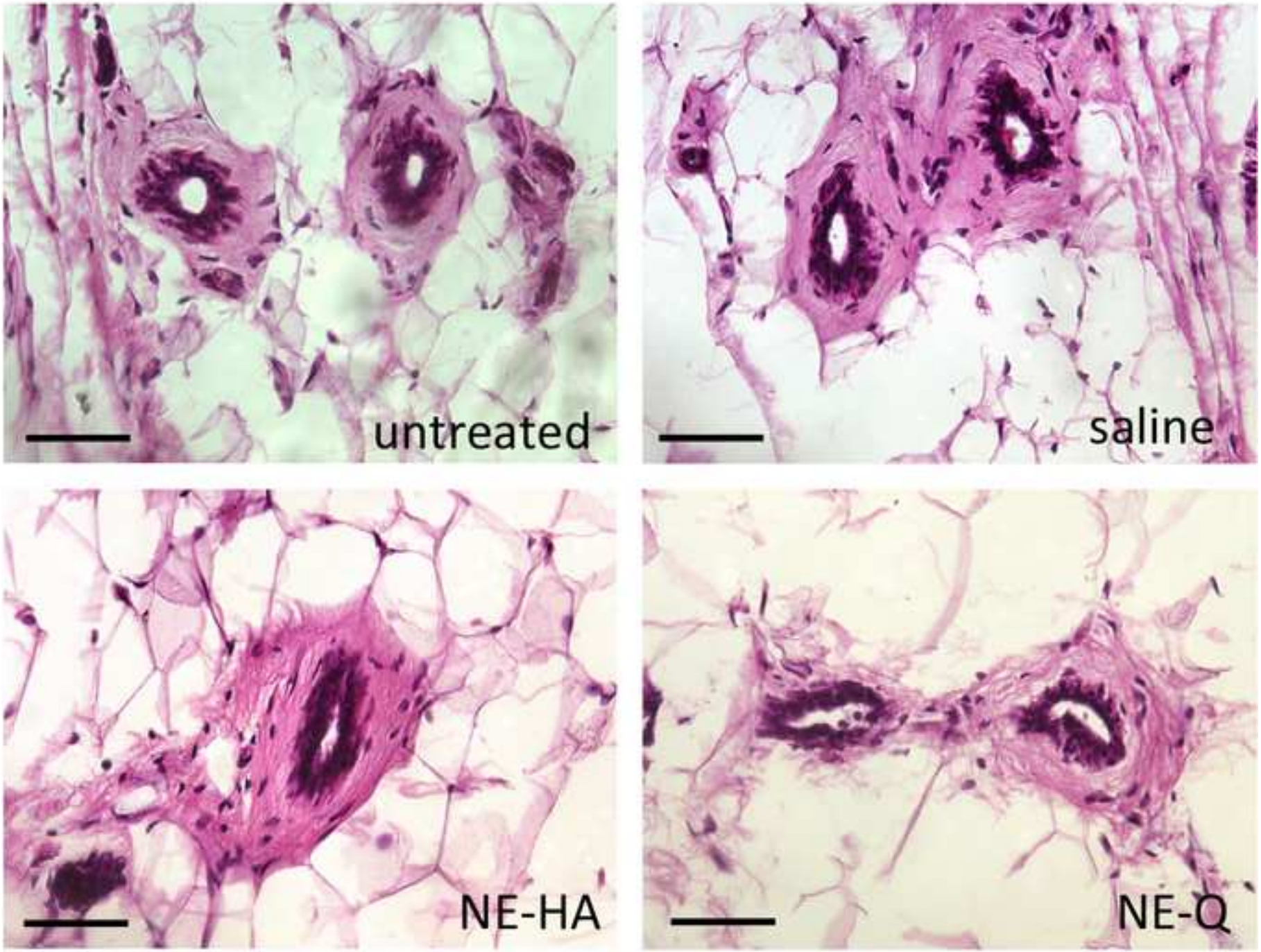

Figure 6

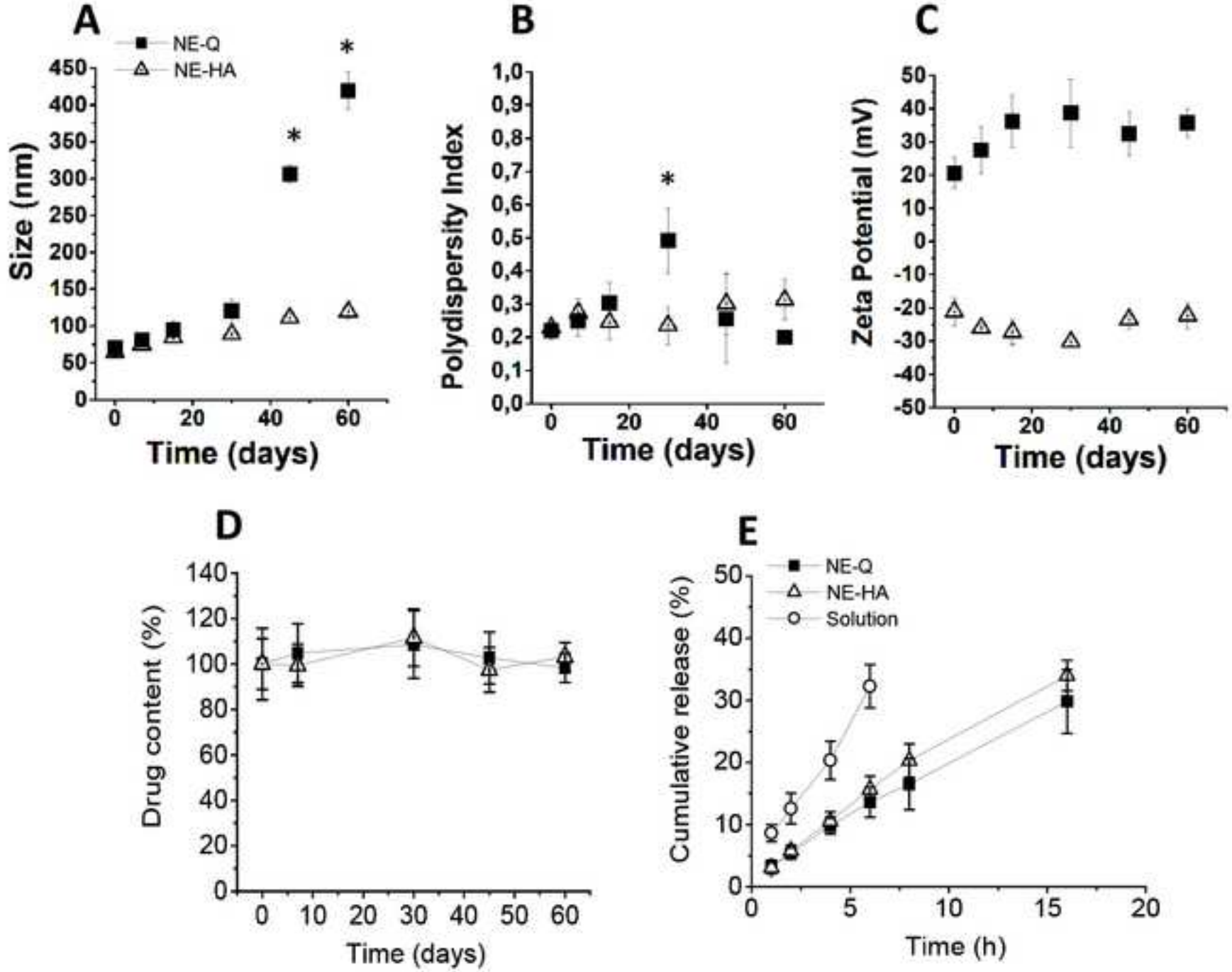
A
NE-Q
NE-HA
Size (nm)
Time (days)
B
Polydispersity Index
Time (days)
C
Zeta Potential (mV)
Time (days)
D
Drug content (%)
Time (days)
E
NE-Q
NE-HA
Solution
Cumulative release (%)
Time (h)

Table(s)

Table 1. Influence of surfactant and aqueous phase content on the physicochemical characteristics of nanoemulsions. The ratio of PC:polysorbate 80:glycerol was 3:1:0.5 (w/w/w), and the aqueous phase was composed of PBS.

Surfactant	**Surfactant: oil phase (w/w)**	**Aqueous phase (%)**	**Size (nm)**	**PDI**	**Zeta potential (mV)**
PC	1:1	66	-----	-----	-----
PC:polysorbate 80:glycerol	1:1	66	-----	-----	-----
PC:polysorbate 80:glycerol	1:1	75	90.7 ± 1.0	0.31 ± 0.01	5.8 ± 2.8
PC:polysorbate 80:glycerol #	1:1	80	76.5 ± 1.2	0.21 ± 0.03 *	6.5 ± 2.7
PC:polysorbate 80:glycerol	2:1	80	73.1 ± 3.3	0.18 ± 0.05 *	6.9 ± 3.0

The symbol # denotes the selected compositon. * $p < 0.05$ compared to the formulation composed of surfactant (PC/polysorbate 80/glycerol):tricaprylin at 1:1 containing 75% of aqueous phase. Use of PC as sole surfactant or PC:polysorbate 80:glycerol with 66% of aqueous phase did not led to nanoemulsion formation.

Table 2. Influence of poloxamer concentration on the physicochemical characteristics of nanoemulsions.

Poloxamer (%, w/w)	**Size (nm)**	**PDI**	**Zeta potential (mV)**
0	76.5 ± 1.2	0.21 ± 0.03	7.6 ± 2.7
0.25	77.3 ± 0.8	0.18 ± 0.02	7.8 ± 2.2
0.50	101.3 ± 2.4	0.21 ± 0.01	7.1 ± 0.6

Table 3. Influence of cetylpyridinium chloride concentration on the physicochemical characteristics of NE-HA.

cetylpyridinium chloride (%, w/w)	**Size (nm)**	**PDI**	**Zeta potential (mV)**
0	66.7 ± 1.5	0.17 ± 0.04	-10.2 ± 3.9
0.01	51.2 ± 1.04	0.22 ± 0.01	-11.4 ± 2.4
0.05	74.4 ± 1.09	0.25 ± 0.01	-8.5 ± 1.1
0.25	45.1 ± 0.14	0.25 ± 0.01	-11.6 ± 0.6
0.50	49.5 ± 0.25	0.22 ± 0.01	+11.3 ± 4.0

Table 4. Influence of chitosan and hyaluronic acid addition on nanoemulsion thermal properties assessed by DSC.

Sample	Heating cycle				Cooling cycle	
	Tg´ (°C)	$T_{onset-fus}$	$T_{peak-fus}$	ΔH_{fus} (J/g)	ΔH_{crys} (J/g)	$T_{peak-crys}$
NE	-45.0	-8.0	-0.8	214.7	185.0	-12.8
NE-HA	-36.0	-2.9	1.4	243.0	197.6	-12.5
NE-Q	-60.0	-9.6	-1.4	179.8	151.4	-20.8

Tg´ = glass transition temperature; $T_{onset-fus}$ = extrapolated onset-temperature of fusion; $T_{peak-fus}$ = endothermic fusion peak temperature; ΔH_{fus} = enthalpy of fusion; ΔH_{crys} = enthalpy of crystallization; $T_{peak-crys}$ = exotermic crystallization peak temperature.

Supplementary Material

Click here to download Supplementary Material: Supplementary Figure.docx

Credit author statement

Carvalho: conceptualization, investigation, methodology, writing- original draft
Salata: investigation, validation
Costa-Fernandez: investigation
Matos: investigation, validation
Chorilli: resources, methodology, writing – review and editing
Araújo: formal analysis, resources, methodology, writing – review and editing
Steiner: funding acquisition, methodology, formal analysis, writing – review and editing
Silveira: methodology, investigation
Costa-Lotufo: conceptualization, writing – review and editing
Lopes: conceptualization, supervision, funding acquisition, formal analysis, methodology, writing- original draft, review and editing.

Supplementary Figures

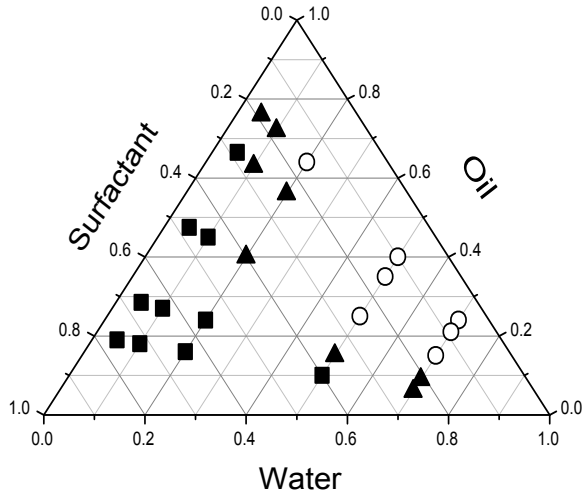

Supplementary Figure 1. Pseudo-ternary phase diagram depicting the relationship between composition and phase behavior of mixtures composed of surfactant (PC:polysorbate 80:glycerol at 3:1:0.5 m/m/m), oil (tricaprylin) and water.

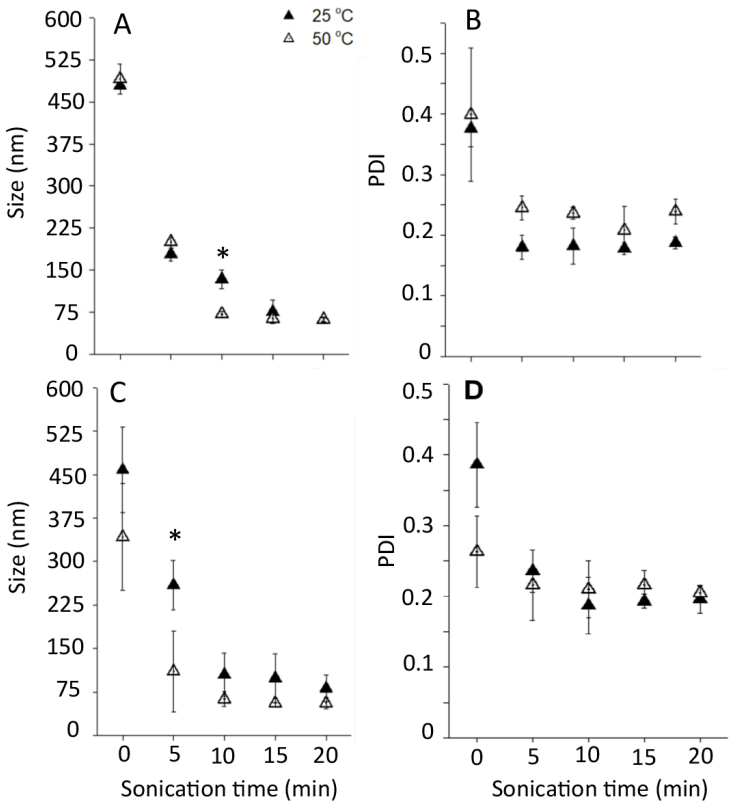

Supplementary Figure 2. Influence of aqueous phase temperature and sonication time on the reduction and distribution of nanoemulsion size. A-B: NE-Q, C-D: NE-HA. At least three batches of each formulation were produced.

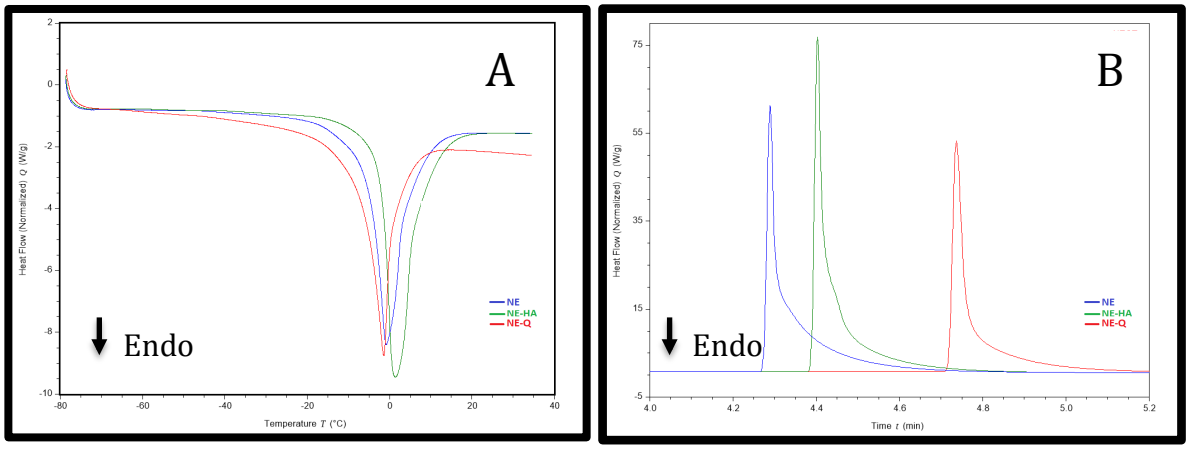

Supplementary Figure 3. DSC curves of heating (A) and cooling (B) cycles for NE (blue), NE-Q (red) and NE-HA (green).

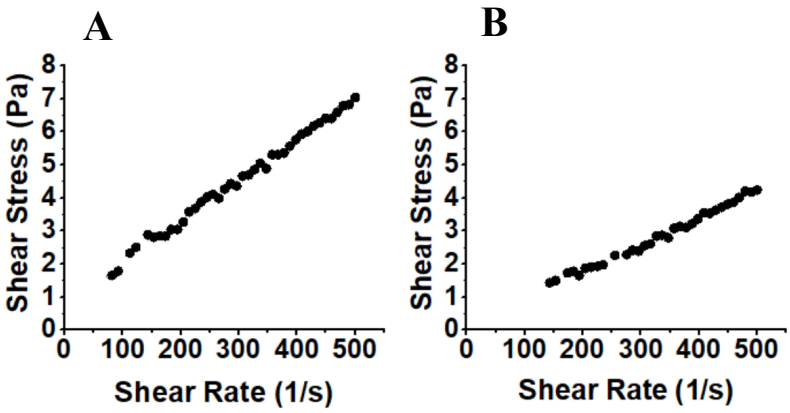

Supplementary Figure 4. Rheological behavior of NE-Q (A) and NE-HA (B).

Supplementary Table 1. Influence of piplartine incorporation on the physicochemical characteristics of nanoemulsions. Data obtained at the day of nanoemulsion preparation.

Formulation	Size (nm)	PDI	Zeta potential (mV)
NC-HA	67.9 ± 0.8	0.22 ± 0.01	-21.2 ± 4.2
NC-Q	70.3 ± 2.0	0.23 ± 0.04	+20.7 ± 3.7